Chemical Engineering Science 277 (2023) 118861

Contents lists available at ScienceDirect

Chemical Engineering Science

journal homepage: www.elsevier.com/locate/ces

Three-dimensional interface structures and characteristics in a stratified gas–liquid pipe flow

Lin-tong Hou [a,b], Meng Yang [a,b], Li-song Wang [a,b], Shuo Liu [a,b,*], Jing-yu Xu [a,b,*]

[a] School of Engineering Sciences, University of Chinese Academy of Sciences, Beijing 100049, RP China
[b] Institute of Mechanics, Chinese Academy of Sciences, Beijing 100190, RP China

ARTICLE INFO

Keywords:
Stratified flow
Acceleration pressure drop
Nonflat assumption
Liquid height
Interface characteristics

ABSTRACT

In this study, the air–water flow in a pipe with a diameter of 100 mm was tested to investigate the three-dimensional (3D) interfacial characteristics of gas–liquid stratified flow in horizontal and slightly inclined pipes. The gas–liquid stratified flow interface exhibited a nonflat phenomenon (concave or convex). In particular, this phenomenon was verified by the transformation of the interface shape when the gas–liquid ratio exceeded 200 and 5 in the horizontal and inclined pipes, respectively. Compared with the flow in the horizontal pipe, the liquid holdup gradually decreased with an increase in the inclination angle in the downward stratified flow, and liquid height changes at the center was slight; however, the convex interface shape was obvious. In addition, the interface exhibited regular fluctuations in the flow direction under fixed operating conditions. Therefore, the hypothesis of a nonflat interface for stratified flow was proposed based on the experimental phenomena, and the interface shape function and flow equations were constructed to predict the degree of interface bending and critical conditions for gas–liquid stratified flow by analyzing the theoretical and influencing factors. The acceleration pressure drop was introduced to quantitatively characterize interfacial fluctuations in the flow direction; therefore, a modified model for nonflat stratified flow was developed. The proposed model could characterize the interface features in both the cross-sectional and flow directions of the pipe and provided a solution for the 3D interface of stratified flow. A comparison with the experimental results revealed that the proposed model performed the prediction satisfactorily. By solving the proposed model, the interfacial information in the pipe cross section and flow direction can be effectively predicted.

1. Introduction

Stratified multiphase flow in pipes is often found in oil and gas transportation systems; it has received increasing attention from both the practical and theoretical points of view, because the stratified flow is a fundamental structure encountered in multiphase systems (Brauner et al., 1995a; Katopodes, 2019). Despite its relative simplicity compared with other flow patterns, stratified flow is, in many cases, the fundamental pattern of multiphase flow transitions; thus, it has a key reference value in studies on the flow stability. Stratified flow is dominated by gravity, which causes liquid to flow in a continuous bottom layer. At low gas velocities, the gas–liquid interface may behave smoothly. While maintaining the liquid flow rate constant, an increase in the gas flow rate leads to the excitation of interfacial waves, whose characteristic properties significantly change with the gas flow rate (Kumar et al., 2021). The transfer of mass, heat, and momentum is strongly influenced by the wave pattern at the interface (Kumar et al., 2021; Cherdantsev et al., 2022).

Owing to the interactions between phases during the stratified flow, the interface is perturbed to generate fluctuations, which increases the flow complexity. Under different flow conditions, clear differences in the stratified flow interface appears, and it is crucial to study the interface characteristics. The discussion of interfacial information generally regards a two-dimensional view of interfacial fluctuations in the flow direction, which originates from the fact that turbulent structures in the high shear region near the wall lift off and impact the interface. The fundamental reason for this is that the velocity of the liquid near the pipe wall is close to zero under the condition of no slip, and the velocity head is converted into static pressure energy, which makes the liquid form a thin layer at the pipe wall, showing the phenomenon of "liquid climbing near the pipe wall." Moreover, under the condition of low liquid holdup, an increasing gas velocity decreases the pressure above the interface, which produces a "suction effect" on the

* Corresponding authors.
E-mail addresses: liushuo@imech.ac.cn (S. Liu), xujingyu@imech.ac.cn (J.-y. Xu).

https://doi.org/10.1016/j.ces.2023.118861
Received 14 February 2023; Received in revised form 16 April 2023; Accepted 7 May 2023
Available online 11 May 2023

Nomenclatures

Variables

A	cross-sectional area, m^2
A_S	the sector area of pipe circle, m^2
A_S'	the sector area of interface circle, m^2
C	fluctuation coefficient
D	pipe diameter, m
D'	diameter of the virtual circle of interface, m
S	wetted parameter, m
$S_\triangle$	triangle area, m^2
U	mean velocity, m/s
u	phase velocity, m/s
h	liquid height, m
h_L	liquid height at the center of pipe section, m
P	pressure, Pa
Q	flow rate, m^3/h
Re	Reynolds number
R'	radius of the interface circle
f	friction factor
m	mass flow rate, kg/s
M	molar mass, kg/mol
R	gas constant, J/kg·K
T	temperature, K
t	time, s
r	radial position, m
g	gravitational acceleration, m/s^2
l	half of wet perimeter length, m
q	liquid–gas ratio
x	axial distance, m
O	interface angle, rad
K	interface curvature, 1/rad
We	Weber number
X^2	Loekhart & Martinelli parameter

Greek symbols

ρ	density, kg/m^3
μ	viscosity, Pa·s
α	angle corresponding to the distance between the two circle centers, rad
ε	gas holdup
1-ε	liquid holdup
τ	shear stress
θ	angle of interface curvature, rad
σ	surface tension coefficient, kg/s^2
β	pipe inclination angle, rad
δ	amplitude of fluctuations, m

Subscripts

G	gas
SG	superficial gas
L	liquid
SL	superficial liquid
TP	two-phase
i	interface
a	acceleration

liquid phase and resulting in a rise in the middle. However, their motion is suppressed in the vertical direction due to gravity and surface tension, and their momentum is redistributed, enhancing the axial fluctuations (Rashidi and Banerjee, 1988). Researchers usually associate this phenomenon with the Kelvin-Helmholtz instability (Barnea, 1991; Barnea and Taitel, 1993; 1994) to further subdivide the category of interfacial fluctuations. Three distinguished states in the stratified wave flow are small-amplitude waves, rolling waves, and atomization associated with droplet detachment from the film (Andritsos and Hanratty, 1987; Tzotzi et al., 2011; Hudaya et al., 2019). The film thickness recordings were statistically analyzed, which determined that small-amplitude waves were periodic and maintained their properties over several bands, whereas large-amplitude waves were more random (Andritsos, 1992; Grue et al., 1999). In the previous numerical simulation study, a similar behavior was observed for wind-generated waves by direct numerical simulation (DNS). Within a short calculation time, the perturbations at the interface show short wavelength and amplitude fluctuations, which then evolve into unstable K-H waves (Lin et al., 2008). This confirms that waves can be generated by turbulence in a pipeline flow. Thus, unsteady interfacial waves excited by turbulence need to develop with a certain entrance length. Therefore, the transient characteristics of the interphase interface during the flow process deserve more attention. Researchers have studied the transition from smooth to wavy stratified flow in pipes with the help of experimental tests, such as laser Doppler anemometers and conductivity probes that measure the internal flow field, to study the stratified flow wave and turbulence structure (Birvalski et al., 2013; Fernandino and Ytrehus, 2008; Belden and Techet, 2011). In addition, particle image velocimetry was applied to determine the flow fields in the liquid and gas phases, and images were used to record the temporal changes in the shape of the transient gas–liquid interface (Birvalski et al., 2014; Sanjou and Nezu, 2011; Fernandino and Ytrehus, 2008). The velocity field was tested by PIV experiments and interpolated into a grid to convert the mean height and mean axial distance to obtain the mean wave amplitude in order to analyze the interfacial dynamics of the stratified/wave flow.

In a stratified flow system, the interface shape determines the contact area between the phases and wettability distribution between them and the pipe wall. The curvature of the interface shape is particularly important in two-phase stratified pipe flows, and it has a key effect on the prediction of flow parameters, such as the phase fraction and pressure drop, and the characterization of the interface (Wijayanta et al., 2022; Banafi and Talaie, 2020). It is worth mentioning that, even in the smooth stratified flow state, the interface shape is not a stable flat surface; however, it displays an interfacial curvature and morphological change in the pipe cross-section. The physical phenomenon of interfacial bending originates from the tendency of wetted fluid to climb over the pipe wall, forming a curved (convex or concave) two-phase partition interface (Gorelik and Brauner, 1999). Stratified flow in liquid–liquid systems with curved interfaces has been observed in experiments (Valle and Kvandal, 1995; Barral and Angeli, 2013; Pitton et al., 2014) and numerical simulations (Ong et al., 1994; Zhan et al., 2018). For two-fluid stratified flow systems with curved interfaces, system energy variation can be used to predict the interface structure and express the characteristic interface curvature (Brauner et al., 1995b, 1996, 1998; Ullmann and Brauner, 2006). It was suggested that the interface shape evolves under different inlet conditions, and investigating the interface shape under fully developed conditions is essential in the numerical simulation of multiphase stratified flows (Berthelsen and Ytrehus, 2007; Brauner et al., 1995a). However, research perspectives and methods associated with the stratified flow at nonflat interfaces need to be further developed, particularly those extending to gas–liquid two-phase flows.

However, an extended safety factor is often chosen to correct the flow in practical applications owing to the complexity of the stratified flow interface. Thus, under certain engineering conditions, the assumption of a flat interface in the pipe cross-section is generally acceptable (Ng et al., 2001; Kumar et al., 2021). Nevertheless, the flat interface assumption is based on low phase velocities, neglecting the surface tension and wall wetting effects, with non-negligible errors in

predictions in the high-viscosity region and at high phase velocities. Consequently, research on the shape of the gas–liquid interface in the pipeline cross-section and interfacial fluctuations in the flow direction urgently requires comprehensive analysis to effectively predict the stratified flow interface characteristics in the three-dimensional (3D) space.

In this study, we investigated the nonflat interfacial phenomena in the gas–liquid stratified flow, constructed an interfacial function model, and modified the flow equations from the perspectives of experimental and theoretical analyses. In the experimental study, the interfacial structure data of the gas–liquid layered flow were obtained. Various statistical parameters were extracted from the accumulated records, and were used to observe the interface characteristics of the flow. In the theoretical study, a two-fluid model was used to simulate the stratified flow with interface bending. In addition, dimensionless parameters were introduced to provide a more complete solution to the multiphase stratified flow problem, including the interface shape, in an attempt to mechanistically explain the causes and influencing factors of the interface shape change and effectively predict the gas–liquid flow interface.

2. Experimental procedure

2.1. Experimental setup and measurements

The data under investigation were acquired during an experimental campaign conducted at the Multiphase Flow Laboratory of the Institute of Mechanics, Chinese Academy of Sciences. The setup consisted of a test bench with an adjustable tilt angle and a U-shaped acrylic pipeline with an internal diameter of 0.1 m. Air and water at atmospheric pressure were used as test fluids. Horizontal and slightly inclined pipe flows were achieved by controlling the experimental bench. The inclination angle of the pipe could be adjusted in the range of 0–5°. A schematic of the test loop is shown in Fig. 1. The total length of the experimental test section of the pipeline is 3.15 m. The test section is 5.75 m away from the entrance of the pipeline, and the minimum length-to-diameter ratio is L/D = 57.5, which can ignore the influence of the entrance effect. The flow structures were directly observed and recorded through a transparent pipe wall.

The test platform consisted of the power, mixing, pipeline, data testing, and data acquisition systems. The experimental techniques, electrical resistance tomography (ERT), pressure sensors, and high-speed cameras were combined to study the air–water flow in pipes. The pressure sensors were arranged at the bottom of the pipe and around the section, and the distance between the two pressure taps along the pipeline length was 1.36 m. Fig. 2 shows the test pipe section. It is worth noting that conventional ERT sensors have limitations in the measurement of thin liquid films (Dong et al., 2006). The composition of the ERT equipment and the measurement mechanism inevitably lead to uneven test sensitivities at various locations in the pipe section. This is manifested by high sensitivity near the wall and low sensitivity near the pipe center, which may lead to amplification of measurement and numerical errors in the reconstructed image (Wang et al., 2002). The sensitivity distribution can be calculated according to the sensitivity theorem (Geselowitz, 1971; Murai and Kagawa, 1985).

In order to ensure the validity of the test data, the conductive resistance loop technique is used in the stratified flow test to overcome the problem of signal overload due to the loss of contact between the electrodes and the conductive phase, and the measurement of thin liquid films is achieved by an algorithm built into the software (Li et al., 2009; Wang and Cilliers, 1999). The use of conductive ring sensors allows for a more uniform sensitivity distribution in the sensing field (Wang et al., 2002; Bolton et al., 2007). Comparison of the test results with the mesh electrode test showed a high degree of agreement (Li et al, 2019a; b), which confirms the uniformity of sensitivity and the validity of the test results using the improved ERT sensor.

The parameters measured in the pipe flow experiment included the

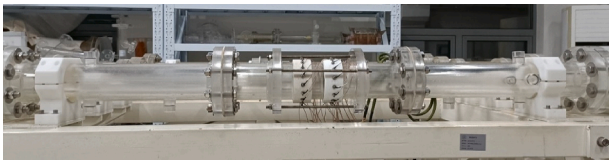

Fig. 2. Test pipe section.

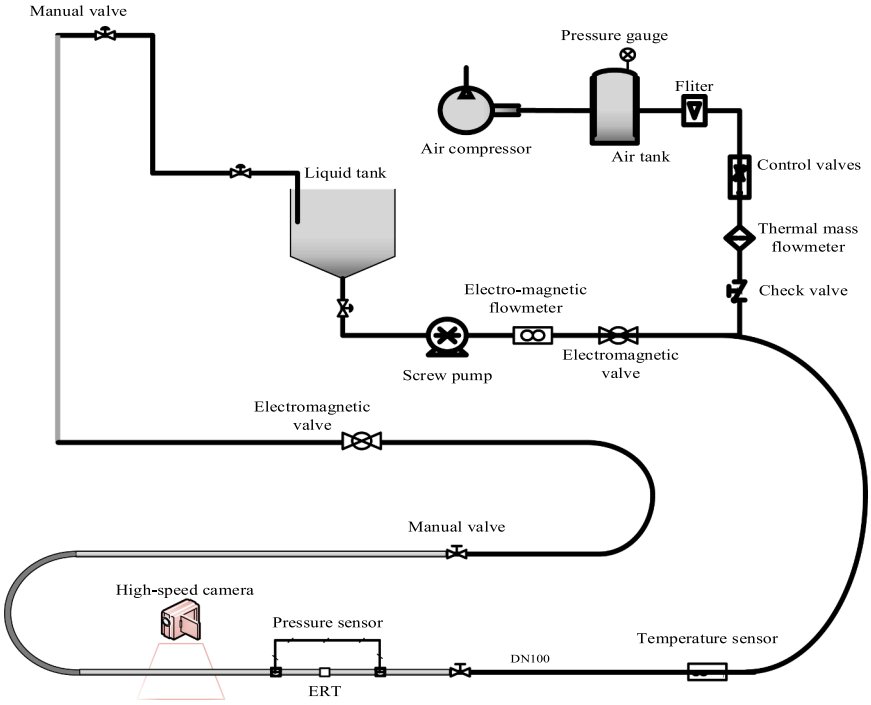

Fig. 1. Schematic of test loop.

superficial gas velocity, superficial liquid velocity, flow pressure gradient, flow pattern, and phase distribution. Table 1 lists the instruments and provides the uncertainty. The detailed parameters of the ERT equipment are listed in Table 2, and the real-time monitoring equipment is shown in Fig. 3. In addition, static calibration of the test equipment was carried out prior to the experiments (Table 3). The pressure sensors were calibrated using ambient air at atmospheric pressure and a hydrostatic water column. On the other hand, the calibration of the ERT sensor was carried out for the test pipe section in the full water condition and in the static gas–liquid stratification condition.

2.2. Test matrices

In this study, experiments were conducted at room temperature in the range of 20–25 °C. Air and water were used as the employed fluids. In the process of gas–liquid two-phase flow, the pressure gradient was measured using pressure sensors, and the phase distribution on the pipe section was monitored by ERT in real time. The liquid superficial velocity (U_{SL}) is in the range of 0.01–0.42 m/s. The gas superficial velocity (U_{SG}) is in the range of 0.09–5.66 m/s. Table 4 lists physical properties of the employed fluids and test conditions. With the help of the parameters in Table 4, the dimensionless Bond number characterizing the effects of surface tension and gravity in this study is calculated to be approximately 330. Fig. 4 shows the distribution of measurement points on the flow pattern map (Barnea, 1987). The experimental data, which were in a clearly stratified flow region, were analyzed. Three repeated experiments were performed under each operating condition. In this study, average values were used.

2.3. Experimental phenomena of gas–liquid interface

In the process of gas–liquid pipe flow, monitoring of the interface shape depends on the ERT reconstruction and data analysis. The contour map in Fig. 5 shows the cross-sectional phase distribution data, which was obtained by measuring the gas–liquid conductivity distribution by ERT and then reconstructed by the internal SBP algorithm. The figure is characterized by the gas volume content as a quantitative representation, where blue area indicates a gas content of 0, which also represents the pure liquid phase region in physics; red area represents a gas content of 1, i.e., the pure gas phase region; and green indicates the gas–liquid phase interface region where the gas content value is between 0 and 1. Moreover, the ERT electrode position did not coincide with the circumferential position of the pipe section owing to the small deflection angle of the pipeline equipment at the butt joint of the ERT device

Table 1
List of instruments.

Measurement parameters	Measuring equipment	Measurement range	Uncertainty
Superficial liquid velocity, U_{SL}	Electromagnetic Flowmeter (KROHN OPTIFLUX4300C)	0–12 m/s	0.2%
Superficial gas velocity, U_{SG}	Rotameter	0–5 m/s	1.5%
Pressure gradient, ΔP	Pressure sensor (Honeywell 40PC15G2A)Data acquisition equipment (NI6210)	0–103 kPa	0.15%
Liquid height at the center of pipe section, h_L	Electrical Resistant Tomography (EIT 3000)	1000 double frames / s	1%
Liquid holdup, ε	Electrical Resistant Tomography (EIT 3000)	1000 double frames / s	1%
Liquid height near the pipe wall, h_L'	Adhesive fiber measurement tool	0–100 mm	0.1%

Table 2
Parameters of EIT 3000.

Parameters	Value
Number of electrodes	16 per plane
Electrode diameter	4 mm
Speed of acquisition for one frame	<20 ms
Max measurement frequency	1000 double frames / s
Cross section pixels	20 × 20
Electrode plane spacing	10 cm

section. As shown in Fig. 5, a certain angle deviation in the cross-section presented by the ERT reconstruction exists, which is shown as non-axisymmetric gas–liquid interface bending. This is because there is a small deflection angle at the junction of the ERT observation pipe and its adjacent experimental pipe section, which causes the observed position of the ERT electrode in the experiment to be inconsistent with the theoretical position. The imaging impact of this hardware problem is eliminated by rotating the ERT cross-sectional distribution data to ensure that the data corresponds to the experimental electrode positions.

The gas–liquid interface of the pipeline section and phase holdup can be obtained by monitoring the phase distribution. Combined with the high-speed video recording of the flow state in real time, the shape of the gas–liquid interface can be further identified, and the change law can be studied. The pipe section data detected by ERT show that the interphase interface in a gas–liquid stratified flow is not a linear plane; however, it often has concave and convex shapes, which are closely associated with the incoming flow conditions and pipe inclinations. Fig. 6 shows the gas–liquid interface shapes captured by ERT under different conditions. where (a) and (b) show the results of the horizontal and downward stratified flow tests, respectively.

Fig. 6 shows the evolution of axial gas–liquid distribution and the variation of radial gas–liquid distributions. Among them, Fig. 6(a) is the concave interface of gas–liquid stratified flow in a horizontal pipe, and Fig. 6(b) indicates the convex interface of gas–liquid stratified flow in a downward inclined pipe. In general, the change of gas–liquid interface shape is primarily affected by the superficial velocity of employed fluids and inclination angle of the pipeline.

The liquid height data of each point on the horizontal radial direction of the pipe section were selected to reflect the gas–liquid distribution on the section. Therefore, the location points in the horizontal radial direction of the pipe section were considered as the horizontal coordinate (r/D) and the dimensionless liquid height (h_L/D) data as the vertical coordinate to form the phase distribution of the pipe section. In this section, the liquid height data of each point on the horizontal axis of the pipeline cross-section is continuously collected and time averaged to obtain the distribution of gas–liquid two-phase on the cross-section, which forms the shape of the gas–liquid interface. In the horizontal pipe flow, the interface shape shows a significant transition under critical conditions with an increase of the superficial gas velocity, as shown in Fig. 7. The experimental data analysis reveals that when the superficial liquid velocity remains unchanged (U_{SL} = 0.021 m/s), the gas velocity gradually increases from 1.415 to 5.659 m/s. When the gas flow rate is low, the gas–liquid interface monitored by ERT is initially concave; when the gas velocity reaches 4.244 m/s, the interface is approximately flat; and when the superficial gas velocity continues to increase, the interface gradually exhibits a convex shape, and the convexity becomes more obvious with the increase in the gas flow rate.

In addition, under some certain conditions, particularly in the downward inclined pipe flow, the gas–liquid stratified flow interface exhibits an evident upward convex shape, and the highest point of the liquid level is at the center of pipe section. However, near the left and right pipe walls, the liquid height rises, as shown in Fig. 8. The experimental results show that when the gas and liquid phases contact in the pipeline at a low speed, an approximately flat interface is formed; however, an increase in the superficial gas velocity causes nonflat

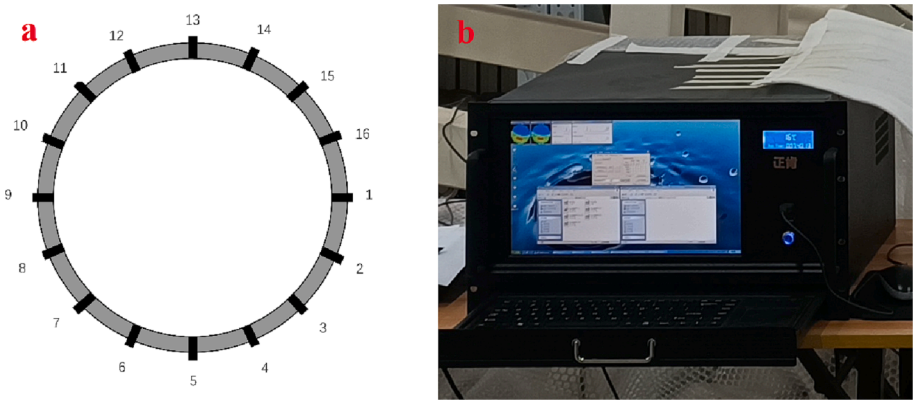

Fig. 3. Experimental ERT: (a) Schematic of electrode distribution, and (b) data acquisition/real-time monitoring system.

Table 3
Calibration of test equipment.

Test equipment	Equipment calibration contents	
	Calibration conditions	Evaluation basis
Pressure sensor	Pipes filled with atmospheric air	The pressure sensor zero output is 0.5 VDC at standard atmospheric pressure
	Horizontal pipes (DN100) in water-filled condition	Calculated hydrostatic pressure of the liquid column at the height of the pipe diameter
Electrical Resistant Tomography (ERT)	Pipeline filled with water (static)	Average gas content of the water-filled section is 0
	Gas-liquid stratification(static)	Conversion of measured values of stationary interface height to average section holdup

phenomena at the gas–liquid interface. The gas–liquid interface bends under the action of the interphase shear force, and it tends to change with the interface velocity. Moreover, under the condition of low liquid holdup, an increasing gas velocity decreases the pressure above the interface, which produces a "suction effect" on the liquid phase and forms a convex interface shape. The reason is that the velocity of the liquid near the pipe wall is close to zero under the condition of no slip, and the velocity head is converted into static pressure energy, which makes the liquid form a thin layer at the pipe wall, showing the phenomenon of "liquid climbing near the pipe wall." As shown in Figs. 7 and 8, at horizontal radial positions above 0.8 or below 0.2, which approximates the region near the pipe wall, the liquid phase has a tendency to climb upward.

Moreover, the experiments and visual monitoring revealed that obvious regular fluctuations appeared at the stratified flow interface in the flow direction. A visualized pipe section with a length of 0.75 m was selected to observe the fluctuation characteristics of its internal stratified flow interface. The interface data proved that the interface differences owing to energy dissipation within the selected pipe section were sufficiently small to be neglected. Therefore, we selected a point on the observed pipe section as the object of the interfacial fluctuation investigation, measured variations in the liquid height at the center of the section, and considered it as the stratified interfacial characteristics of the entire observed section. Although the assumptions caused errors, the analysis proved that this bias threshold was acceptable in this study.

During the experiment, variations in the liquid height at the center of the fixed section was obtained by visual recording. When the superficial velocity of the liquid phase was 0.021 m/s, after a stable flow was formed, the data of the interface of the observation point for a period of time were recorded, as shown in Fig. 9. Fig. 9(a) and (b) give the test results of the interface position for different gas phase apparent velocities at a fixed liquid phase apparent velocity. The observation section was selected at 7.7 m from the inlet of the mixed incoming fluid to ensure that the flow has reached full development here. The curves included in Fig. 9 represent the height variation of the gas–liquid interface at the observed section at different times, while the corresponding photographs under the curves show the real-time record of the gas–liquid flow in the observed pipe section during the observation time. It is important to explain that in a steadily developing air–water stratified flow, the flow attenuation is assumed to be negligible for a short period of time. The information of the interface fluctuations is shown qualitatively and compared with the corresponding visualized images;

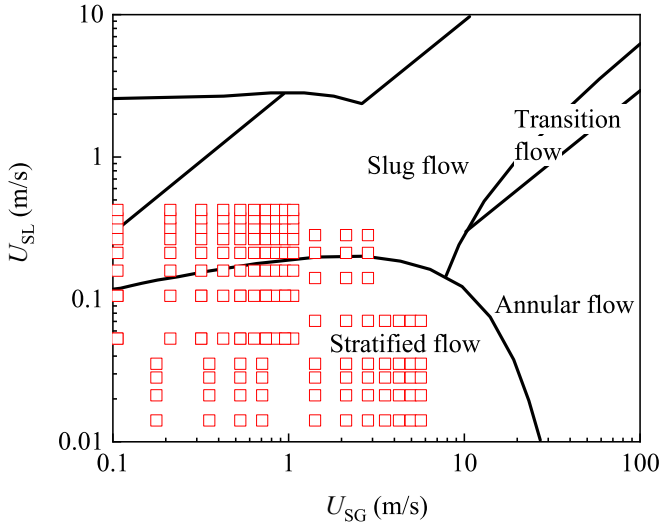

Fig. 4. Distribution of measurement points on the flow patterns map.

Table 4
Experimental test matrix.

Pipe angle (°)	Diameter (mm)	Operating fluids	Superficial velocity (m/s)	Density (kg/m^3)	Viscosity (Pa•s)	Surface tension (N/m)	Flow pattern
0,1,2,4	100	air–water	$0.01 \le U_{SL} \le 0.42$ $0.09 \le U_{SG} \le 5.66$	$\rho_L = 999.126$ $\rho_G = 1.226$	$\mu_L = 0.001$ $\mu_G = 0.000018$	0.073	stratified flow

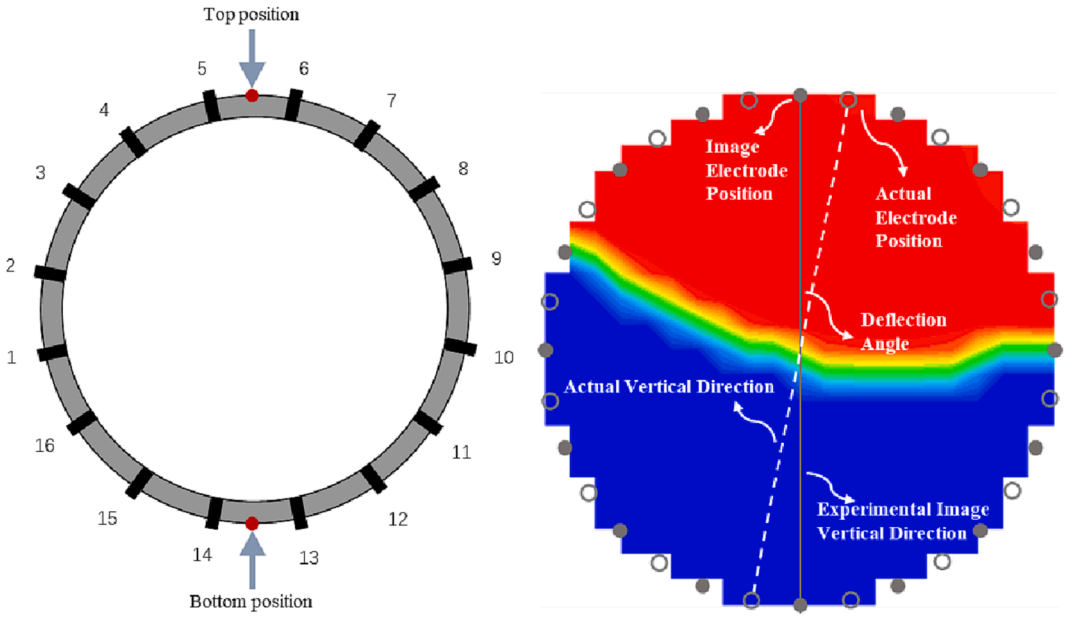

Fig. 5. Schematic of pipe section electrodes layout.

the results of the interface fluctuations in the flow direction were satisfactorily consistent.

The gas–liquid ratio is often used in gas–liquid two-phase flow studies to analyze the flow characteristics and characterize the effect of gas–liquid proportion on the flow system. The gas–liquid ratio is defined as the ratio of the superficial gas and liquid velocity, expressed as U_{SG}/U_{SL}. As shown in Fig. 9, at a low gas–liquid ratio, the interfacial fluctuation phenomenon is enhanced with an increasing superficial gas velocity, whereas a further increase in the velocity of the gas phase increases the frequency of interfacial waves, decreases the wave amplitude, and decreases the liquid height gradually. Furthermore, at a high gas–liquid ratio, the gas–liquid interface wave amplitude is small and appears as a ripple. As the superficial liquid velocity increases, the wave amplitude increases, frequency of interfacial waves decreases, and liquid height increases.

2.4. Analysis and discussion

The data collected by ERT were analyzed considering the liquid height, average phase holdup of the cross-section, and gas–liquid distribution in the axial direction of the pipeline to further explore the characteristics of gas–liquid stratified flow. The interface fluctuations measured by ERT electrodes are qualitatively consistent with the actual fluctuations observed in the video recordings (Fig. 9). However, there are still some errors compared to the actual values, which can be caused by factors such as the number of electrodes, sensing accuracy, etc., in addition to our assumptions (Guo et al., 2020).

During data analysis, the measurement error of the parameters and the error propagation of the derived function are comprehensively evaluated. According to error propagation proposed by Bevington and Robinson (2003), error transfer analysis is carried out on the indirect measurement parameters derived from the direct measurement parameters in the study.

Suppose the indirect measurement parameter is $f = f(x,y,\ldots,n)$, the error propagation formula is defined as:

$$\sigma_f = \sqrt{\sigma_x^2\left(\frac{\partial f}{\partial x}\right)^2 + \sigma_y^2\left(\frac{\partial f}{\partial y}\right)^2 + \ldots + \sigma_n^2\left(\frac{\partial f}{\partial n}\right)^2} \tag{1}$$

where σ_f is the error of the indirectly measured parameter.σ_x, $\sigma_y, \ldots,$ σ_n represent the errors of the direct measurement parameters x, y, ⋯, n that make up the parameter f. It should be noted that the error of direct measurement parameters is calculated by the standard error of the average value:

$$\sigma_{x,y,\ldots,n} = \sqrt{\frac{\sum_{i=1}^{N}(x_i - \bar{x})^2}{N(N-1)}} \tag{2}$$

where N represents the number of standard repeated experiments.

2.4.1. Liquid height at the center of cross-section

In the flat interface assumption of gas–liquid stratified flow, the average liquid height is a key parameter for characterizing two-phase flow. Moreover, under the nonflat assumption, the average liquid height has limitations in describing the shape of gas–liquid interface. Therefore, the liquid height at the center of pipeline cross-section was used as a parameter to discuss its variation trend and influencing factors and considering it as an effective approach to explore the gas–liquid flow state under the nonflat assumption.

The acquisition of the liquid height at the center of the pipe cross-section was carried out by indirect measurement methods. The ERT reconstructed phase distribution is combined with the liquid level visualization data near the pipe wall to determine the specific location of the gas–liquid interfaces in the transition zone reconstructed by the ERT algorithm, which is then converted to the center of the section using interpolation to obtain the liquid height data at the center. Fig. 10 shows variations of the liquid height at the center of cross-section.

The vertical axis in Fig. 10 represents the dimensionless liquid height, which is expressed as the ratio of the liquid height at the center of pipe section to the pipe diameter, and the horizontal axis represents the superficial gas velocity. Fig. 10(a) and (b) show the variation of liquid height for different gas and liquid velocity conditions of stratified flow. The results show that when the superficial liquid velocity is fixed, the liquid height at the center of pipe cross-section decreases with an increase in the gas velocity, which is consistent for different liquid-phase superficial velocity conditions. The reason for this is that as the superficial gas velocity increases, the gas occupies more space in the pipe cross-section and the accumulation of the liquid phase decreases, leading to a decrease in the liquid height.

Similarly, the influence of the liquid flow conditions on the stratified flow is non-negligible. When the superficial gas velocity is constant and

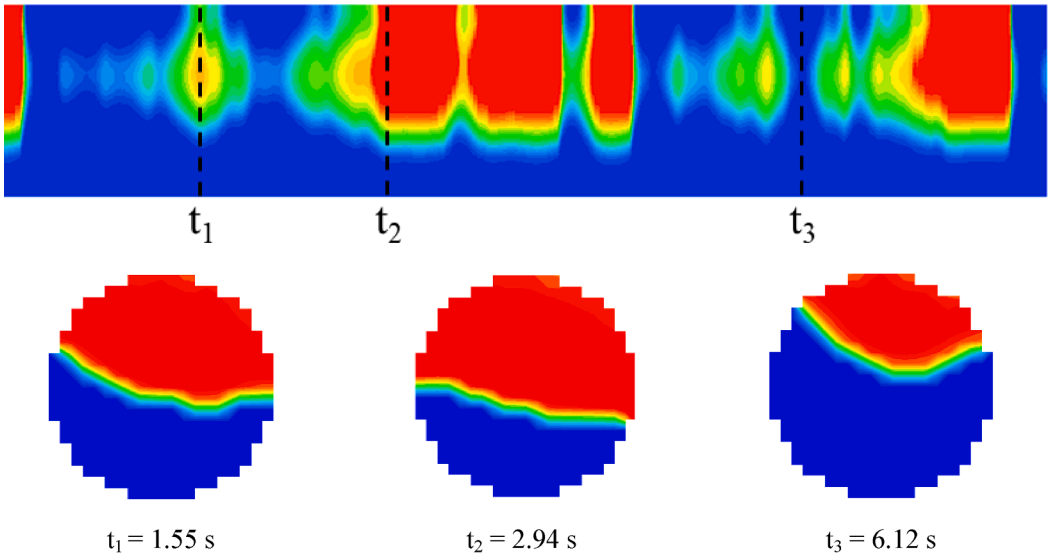

(a) Gas-liquid concave interface (U_{SG} = 0.11 m/s, U_{SL} = 0.05 m/s; β = 0°)

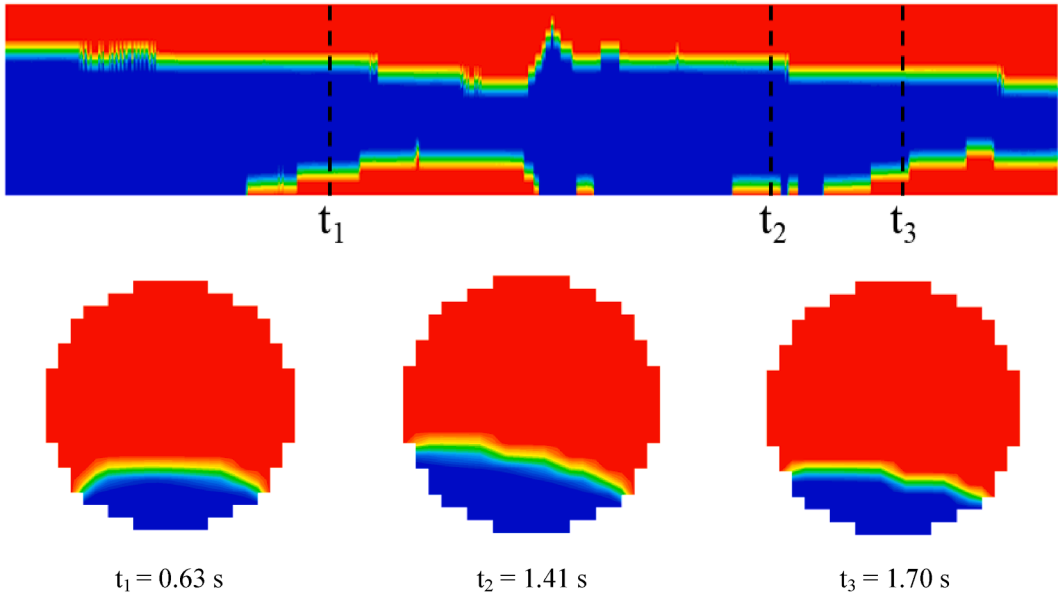

(b) Gas-liquid concave interface (U_{SG} = 0.09 m/s, U_{SL} = 0.21 m/s; β = 2°)

Fig. 6. Shape of gas–liquid interface under different operating conditions.

the liquid velocity is increased, the liquid height shows a tendency to rise gradually, as shown in Fig. 11. It is worth noting that the small variation of the gas at higher gas-to-liquid velocity ratios does not have a significant effect on the liquid surface height. This phenomenon occurs especially at $U_{SL} < 0.025$ m/s, whereas the effect of liquid gravity increases with an increase in the superficial liquid velocity, leading to a significant accumulation of the liquid height.

Fig. 12 shows the trend of power function distribution of the liquid height with the variation of liquid–gas velocity ratio. Specifically, the growth rate of the liquid height at the center of the pipe decreases as the liquid-gas velocity ratio increases. This is because under high liquid–gas velocity ratio conditions, the effect of the interphase shear remains secondary to the effect of gravity, and its effect on the two-phase flow is difficult to detect by ERT. However, if the superficial gas velocity is further increased, the interfacial effect becomes increasingly significant, which promotes variations of the liquid height in the pipe.

Moreover, variations in the liquid height at the center of pipe section in both horizontal and inclined downward stratified flows are shown in Fig. 13. The results reveal that the stratified flow liquid height is influenced by the velocity of the gas and liquid phases in both the inclined and horizontal pipes; however, the stratified flow characteristics are significantly affected by the inclination angle owing to the participation of gravity.

In the inclined downward stratified flow, variations in the liquid height at the center of pipe cross-section was similar to that in the horizontal pipe, indicating a positive correlation with the superficial velocity of the liquid phase and a negative correlation with the superficial gas velocity. The superficial liquid velocity had a more significant

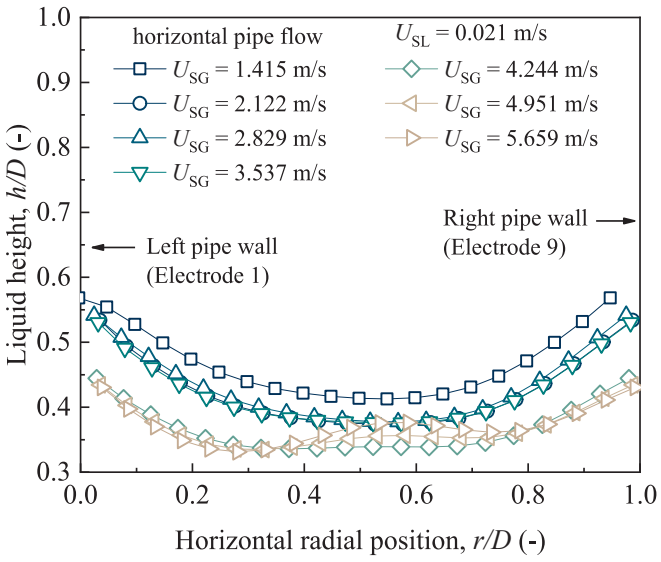

Fig. 7. Interface shape of gas–liquid stratified flow in the horizontal pipeline.

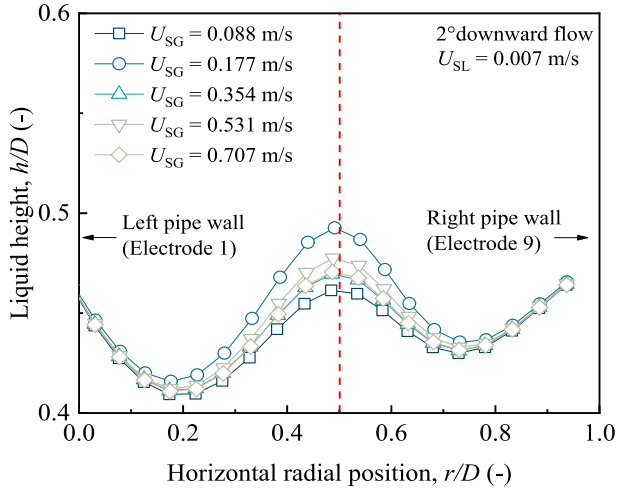

Fig. 8. Interface shape of gas–liquid stratified flow in the downward pipeline.

effect on the liquid height and liquid holdup, as shown in Fig. 13. Fig. 13 (a) shows a significant difference between the liquid height of the 2° downward stratified flow and that of the horizontal flow under the same incoming flow conditions, and the difference between the two diminishes as the superficial velocity of the gas phase increases. Whereas the difference in liquid height caused by tilting 1° and 2° downward in Fig. 13(b) is smaller. This indicates that the influence of the pipe inclination angle on the flow is not dominant in the current operating conditions. The reason may be that although the gravitational effect formed by the inclination angle has an effect on the layered flow characteristics, at the same time, the gas–liquid velocity ratio determines the interphase forces, so exploring the flow state requires a comprehensive consideration of the synergistic effects of gravity and interphase shear forces.

Fig. 14 shows a clear difference in the position of the gas–liquid interface in the vertical radial direction of the pipe cross-section that occurs with the variation of pipe inclinations in the stratified flow. The results of Figs. 13 and 14 show that at the same incoming phase velocity, the position of the gas–liquid interface gradually decreases with an increasing pipe inclination angle and is significantly lower than that of the stratified flow in the horizontal pipe. Moreover, in the stratified flow of a slightly inclined downward pipe (an inclination angle less than 5°), the variation of pipe inclination redistributes the fluids. Under the effect of gravity, the velocity of liquid phase increases and the slippage between gas and liquid decreases. The calculation of liquid holdup in the stratified flow can be expressed as

$$1-\varepsilon=\frac{A_L}{A_L+A_G}=\frac{Q_L/U_L}{Q_L/U_L+Q_G/U_G}=\frac{1}{1+\frac{Q_G}{Q_L}\frac{U_L}{U_G}} \tag{3}$$

where 1-ε is the liquid holdup, A is the area of the pipe cross-section occupied by a single phase, Q represents the flow rate, and U is the velocity. The subscripts L and G denote separate liquid and gas phases, respectively.

Eq. (3) shows that for a certain gas–liquid ratio, a smaller degree of gas–liquid slippage decreases the value of the holdup and liquid height. Specifically, when the volume flow rates of gas and liquid are basically constant, with the increase in the inclination of the pipeline, the velocity of the liquid phase increases under the effect of gravity, resulting in a decrease in the velocity difference between the gas and liquid phases. This will lead to a weakening of the slip between the two phases and an increase in the liquid–gas velocity ratio. According to Eq. (3), the cross-sectional liquid holdup of the stratified flow decreases accordingly, and therefore the liquid height decreases. Collectively, this can explain the slight decrease in the stratified flow liquid height with an increase in the pipe inclination angle within a certain range.

Variations in the liquid height at the center of pipe cross-section with the volume flow rate of the employed fluids were obtained by analyzing the experimental data, as shown in Fig. 15. The results clearly show that the liquid height was negatively correlated with the gas volume flow rate and positively correlated with that of the liquid. This is because an increase in gas flow will occupy more space in the pipe cross-section; thus, the liquid level accumulation decreases and liquid height decreases. The dimensionless liquid heights for different flow conditions are analyzed in Fig. 15 in an attempt to characterize the sensitivity of the liquid height by the slope of the fitted straight line to the gas volume

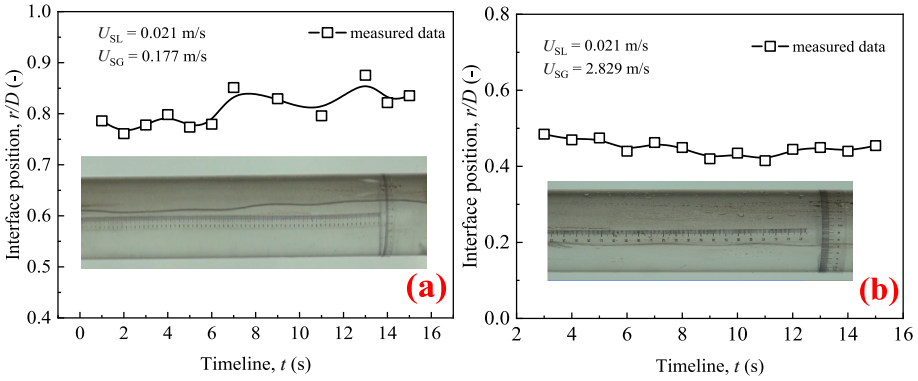

Fig. 9. Interfacial fluctuations in the flow direction.

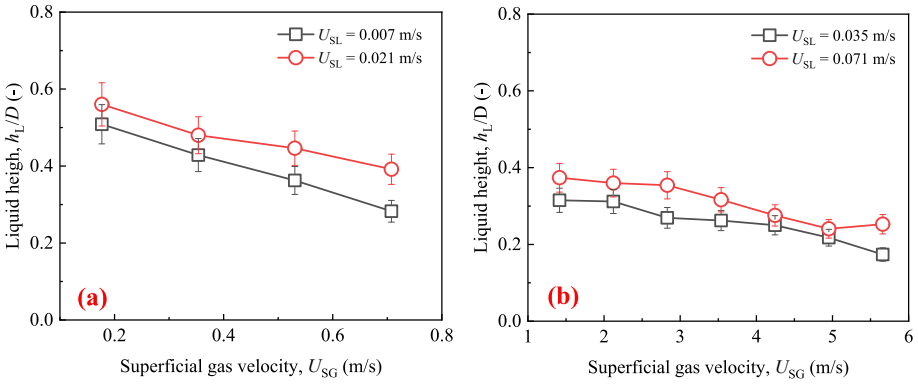

Fig. 10. Liquid height of the horizontal pipeline.

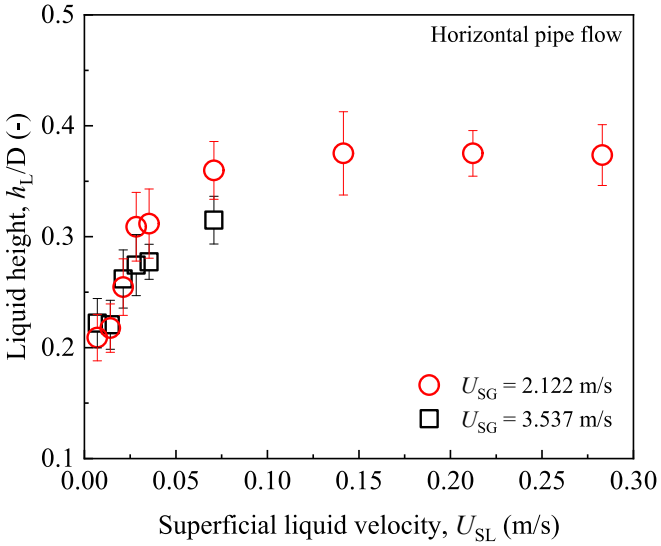

Fig. 11. Variation of liquid height at the center of pipe section with superficial liquid velocity.

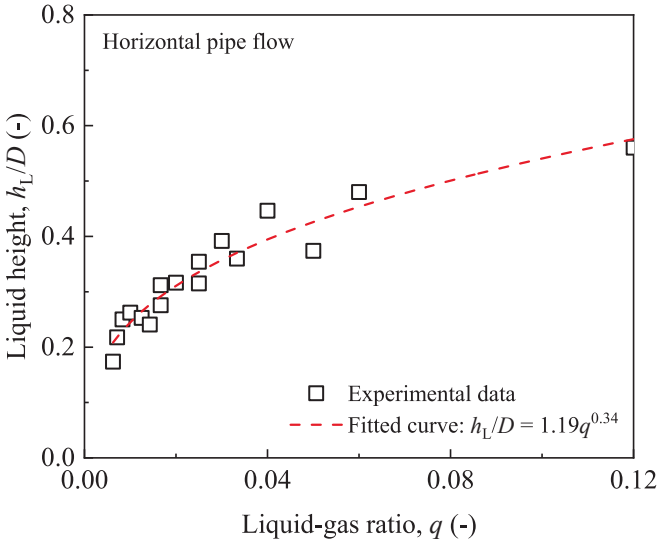

Fig. 12. Relationship between liquid height and liquid–gas velocity ratio.

flow rate. The result indicates that at a low liquid-phase flow velocity, the liquid height is affected by the gas with a significant sensitivity, which is also demonstrated in Fig. 11.

2.4.2. *Shape of gas–liquid interface*

It is confirmed by indoor experiments that the gas–liquid interface of stratified flow in the pipe is not a uniform flat shape, but more often shows a concave or convex curved interface. And with the change of incoming flow conditions, the interface shape will show a regular transformation. As shown in Fig. 16. The gas–liquid interface maintained a concave shape when the liquid phase flow rate was high. Furthermore, when the liquid velocity is lower than 0.07 m/s, the stratified flow interface exhibits a tendency of convex shape at a fixed gas velocity of 0.35 m/s. In general, when the gas–liquid ratio increases to five, the stratified flow interface begins to transform, and this transformation is produced by the synergistic effect of the gravity and interfacial shear force in the pipeline. It should be explained that in Fig. 16, r/D = 0 represents the left wall surface of the pipe section and r/D = 1 represents the right wall surface. Due to the small deviation in the placement of ERT electrodes along the pipe section, the electrodes do not appear exactly at the left and right endpoints of the pipe section, so there will be an angular deviation in the overall imaging. All curve data representing the interface shape in this work have been rotationally corrected to ensure accurate correspondence between the acquired data and the physical location. This results in curves that do not start and end at r/D = 0 and r/D = 1.

The difference in the stratified flow interface is mainly determined by the liquid height at the center (r/D = 0.5) and the curvature of the interface curve. Fig. 17 illustrates that the inclination angle has a significant effect on the interface of stratified flow phase distribution in the pipe under the same inlet conditions. As shown in Fig. 17, the horizontal and inclined stratified flow characteristics were compared under the same gas and liquid velocity conditions. The liquid height of the inclined downward stratified flow is slightly lower than that of the in the horizontal pipe due to the influence of gravity component, indicating that the involvement of gravity has a suppressive effect on the accumulation of liquid height. Furthermore, the results of the study also show the effect of tilt angle on the interface shape. The interface shape transition method is analyzed in conjunction with Fig. 16 to further guide the construction of the interface shape function. In addition, the liquid height data at different locations in the pipe cross-section can corroborate the nonflat characteristics of stratified flow in the pipe, as presented in Fig. 18. The data of liquid height at the center of pipe section and near the wall clearly show the differences under different operating conditions. The black and red curves in the figure represent the time-averaged liquid height at the center of the pipe cross-section and near the pipe wall, respectively, for different incoming flow conditions. Specifically, when the red curve is higher than the black one under the same working condition, it means that the liquid height near the pipe wall is higher

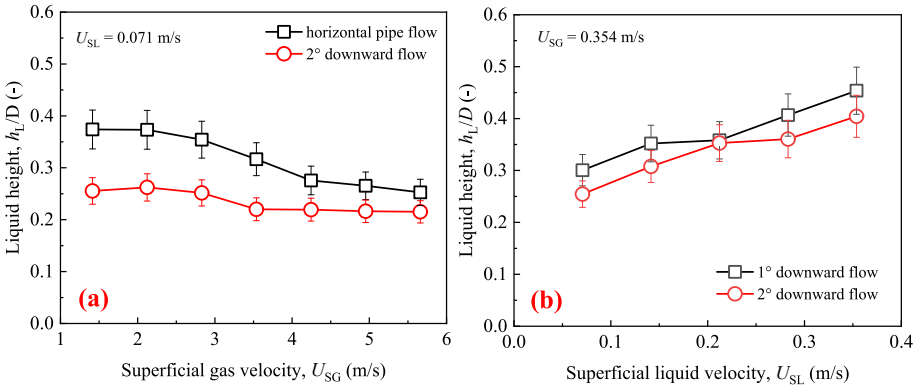

Fig. 13. Variations of liquid height in stratified flow at different pipe inclination angles.

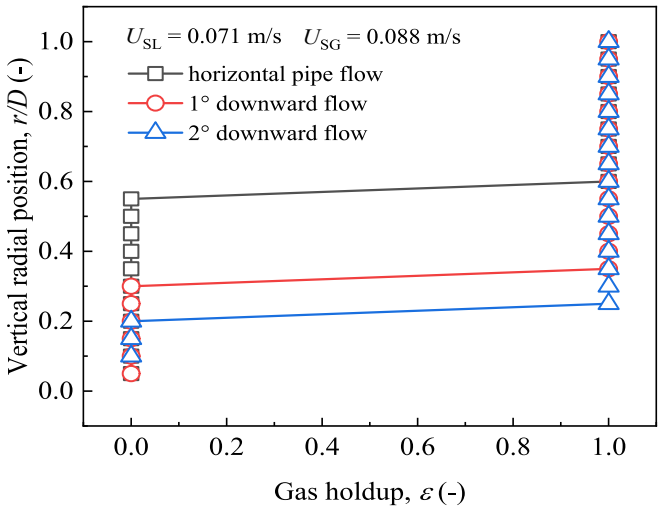

Fig. 14. Liquid height at the center of pipe section under different pipe inclination angle conditions.

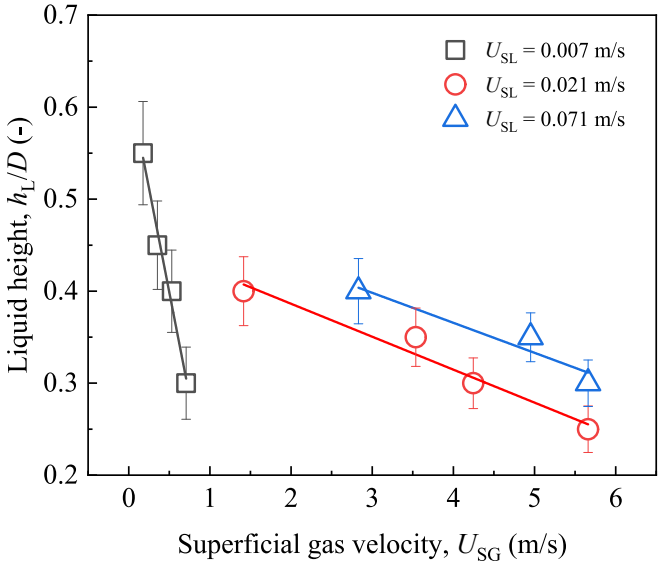

Fig. 15. Relationship between the liquid height and superficial velocity.

than at the center of the pipe, as shown in the schematic diagram of the left cross section in Fig. 18, which shows a concave gas–liquid surface shape; conversely, it shows a convex interface shape as shown on the

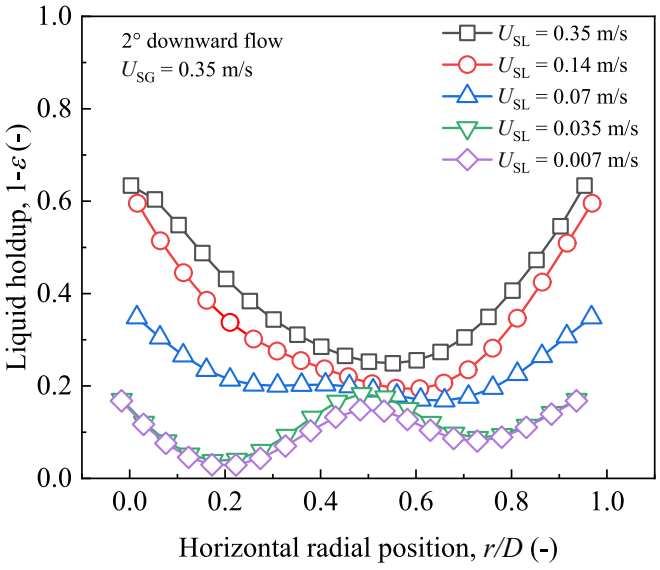

Fig. 16. Interface shape of gas–liquid stratified flow under different operating conditions in the downward pipeline.

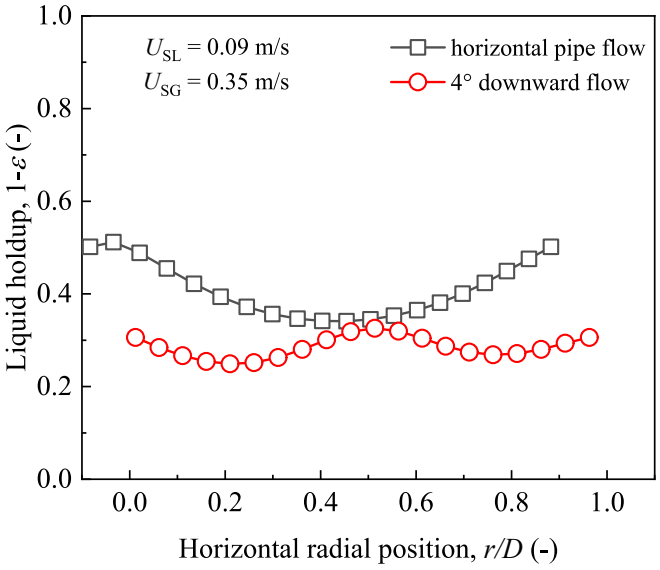

Fig. 17. Variation of stratified flow interface shape with pipe inclination angle.

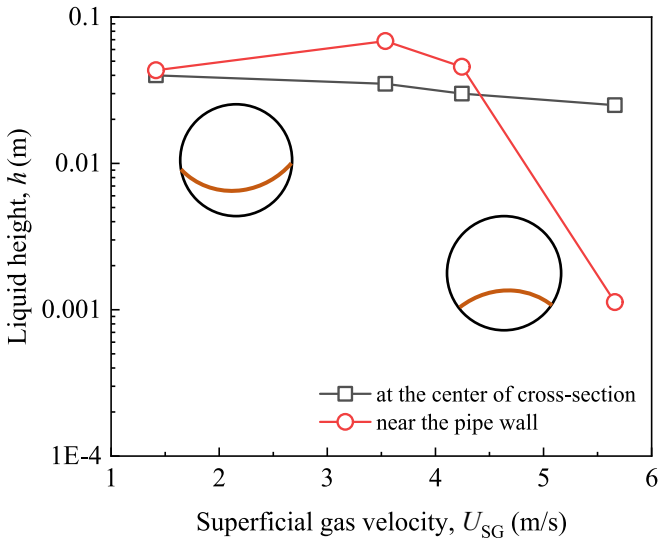

Fig. 18. Comparison of liquid height at different locations on the pipe cross-section.

right side. These data help further examine the evolution of interface shape.

2.4.3. *Liquid holdup characteristics of stratified flow*

The average liquid holdup is a key parameter for characterizing stratified flow properties. In this study, we collated and analyzed the test data to explore the variation rules and impact factors of stratified flow in the horizontal and inclined pipelines. The results show that the liquid holdup of gas–liquid stratified flow is directly related to the incoming flow velocity and pipe inclination angle. Fig. 19 shows liquid holdup variations with phase velocity in the horizontal pipe. It can be observed that the liquid holdup first sharply decreases in a linear manner with an increase in the superficial gas velocity, and then the decrease slows down significantly or even stabilizes. In addition, the liquid holdup has a high sensitivity to gas at superficial gas velocities below 1 m/s; this phenomenon exists under different superficial liquid velocities because when the superficial gas velocity is low, the gas–liquid ratio is less than 1, and a higher liquid height is formed in the pipeline. Simultaneously, because the initial superficial velocity of the liquid phase slightly differs from the superficial gas velocity, when the gas flow rate increases further, it is bound to occupy the space of original liquid phase. When the superficial gas velocity slightly increases, the gas–liquid ratio becomes greater than 1 and continues to grow; subsequently, the cross-section of pipeline exhibits a sharp decrease in the liquid holdup, allowing the gas phase to occupy a larger space to ensure that the gas phase flow obstruction is reduced and the cross-sectional throughput is increased. Nevertheless, when the superficial velocity of gas phase exceeds 1 m/s, the gas–liquid ratio increases to become greater than 5. At this stage, the liquid height is extremely small for the obstruction of gas flow, and changes in the liquid holdup slows down or even fluctuates near an equilibrium value.

The analysis shows that the gas–liquid ratio has a significant effect on the stratified flow characteristics. Fig. 20 shows variations of liquid holdup owing to the increase in the gas–liquid ratio from 10 to 70 under low liquid volume conditions. It is clear that the liquid holdup exhibits an overall decreasing trend with an increasing gas–liquid ratio, and this trend remains consistent for different superficial liquid velocities. Moreover, an increase in the gas-phase velocity yields a minimum holdup value at a certain gas–liquid ratio, and then slightly increases; this minimum value is positively correlated with the superficial liquid velocity, because the gas–liquid interaction is the strongest at this gas–liquid ratio, which is reflected as the turning point of the liquid holdup.

For a downward stratified flow, variations in the liquid holdup were not obvious when the superficial velocity of gas phase was small; however, it abruptly dropped when the superficial gas velocity approached 1 m/s, and gradually stabilized as the gas velocity continued to increase, as shown in Fig. 21. In the downward pipeline, the liquid phase is subject to enhanced gravity; in addition, increasing the gas flow rate has a small effect on the liquid holdup when the gas velocity is not large and the liquid surface condition formed by the gravity effect dominates. However, when the superficial velocity of gas phase exceeded the critical interval, the effect of gas gradually appears and exceeds the effect of gravity, which manifests as a sudden decrease in the liquid holdup. At this stage, under the synergistic effect of gravity and interface shear, the stratified flow liquid height is maintained at a low level, and the rate of reduction of the holdup is slowed down by further increase of gas conditions on a small scale. Fig. 22 shows a positive correlation between the stratified flow holdup and superficial liquid velocity for different inclined pipe conditions. In addition, the gravity effect caused by a larger tilt pipe angle is obvious, which in turn reduces the stratified flow

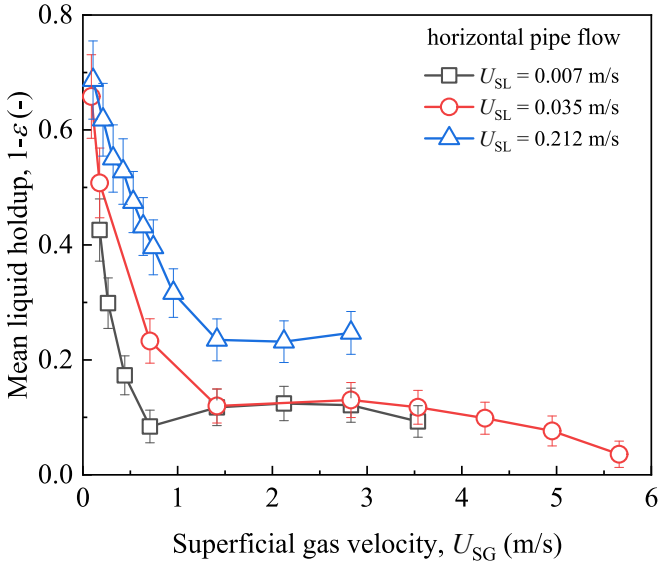

Fig. 19. Variations of liquid holdup in terms of superficial gas velocity.

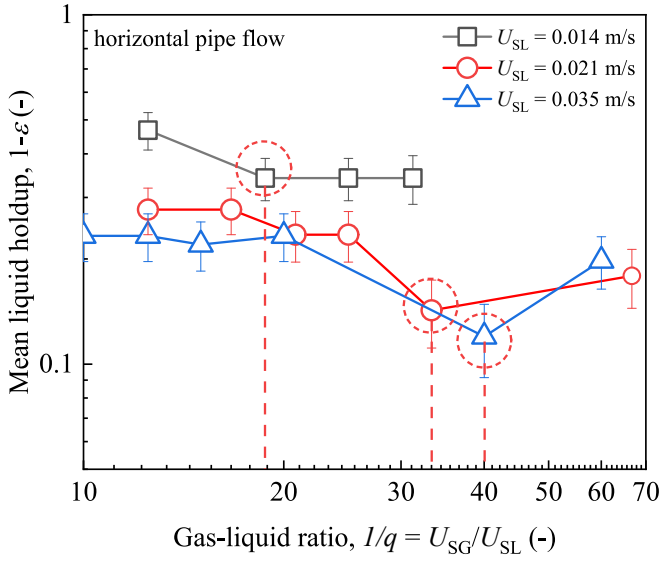

Fig. 20. Effect of gas–liquid ratio on the liquid holdup of horizontal stratified flow.

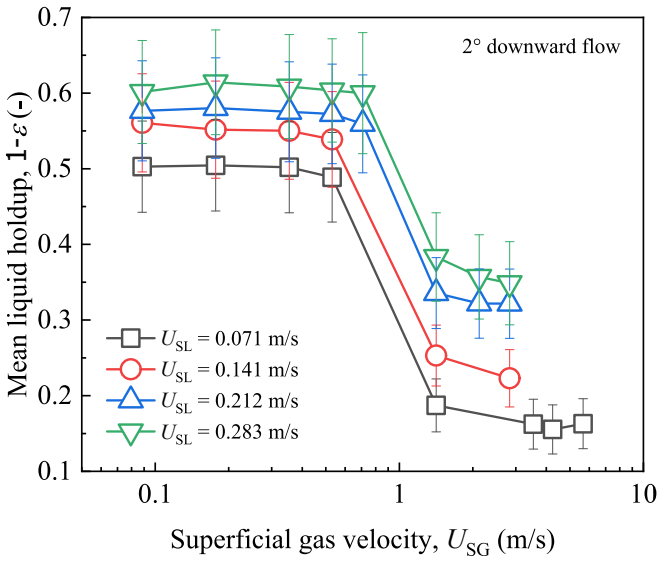

Fig. 21. Liquid holdup in terms of the phase velocity in downward stratified flow.

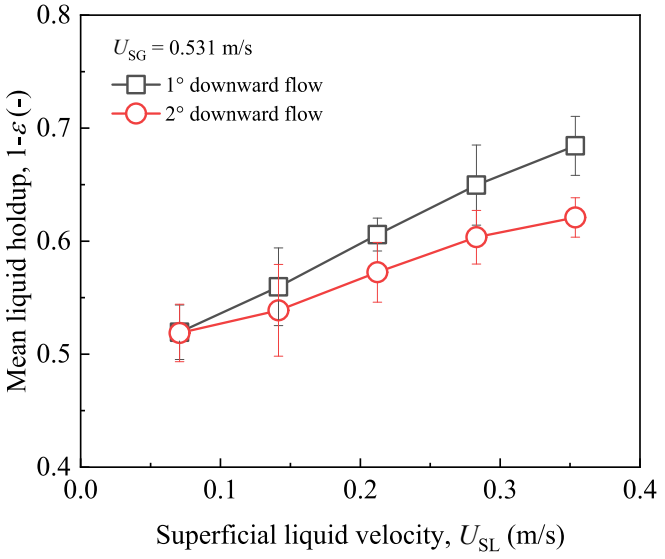

Fig. 22. Relationship between the liquid holdup and superficial liquid velocity at different pipe inclinations.

holdup.

3. Nonflat interface modeling of stratified flow

This study primarily focuses on the gas–liquid stratified flow, monitoring variations in two-phase flow parameters, and obtaining interface characteristics of the gas–liquid stratified flow by analyzing the experimental data. The results of the stratified flow experiments confirmed the characteristic nonflat structure of the interface from the side. The analysis shows that change in curvature changes of the stratified flow interface is not obvious under certain operating conditions, particularly at low liquid holdup. Therefore, combined with the experimental phenomena, it is appropriate to use the double-circle model to characterize the gas–liquid stratified flow interface (Chen et al., 1997). Further expansion based on the double-circle model to cover concave and convex interface shape characteristics is shown in Fig. 23.

The Double-circle model was used to simulate the geometric relationship between the section of the gas–liquid flow pipeline and virtual circle at the interface. Two parameters were introduced: the angle of the interface curvature, θ, and liquid height at the center of pipe section, h_L. Moreover, the interface shape can be determined using the angle of interface curvature, that is, when the gas–liquid interface is concave or convex, the angle of the interface curvature is greater or less than π, respectively.

Fig. 23 gives the position relationship between the two types of pipeline circles and virtual circles, where the black solid circles indicate pipeline circles and the red dashed circles represent interface virtual circles. N_1 and N_2 are used to represent the center of pipe circle and interface virtual circle, respectively, and the corresponding angles are shown in Fig. 23; D and D' represent the corresponding diameters. Fig. 23 shows the geometric relationship and parameter representation of the two circles. It can be seen that the relationship between the considered angles satisfies

$$2O' = 2|\theta - \pi| \tag{4}$$

Using the law of Sines, the diameter expression of the virtual circle formed by the interface curve can be expressed as follows:

$$\frac{D'/2}{\sin(O)} = \frac{D/2}{\sin|\theta - \pi|} \tag{5}$$

The curvature of the interface curve can be expressed as

$$K = \frac{1}{R'} = \frac{2\sin|\theta - \pi|}{D\sin(O)} \tag{6}$$

By combining Eq. (6) with the Double-circle model in Fig. 23, the angle α corresponding to the distance between the two circle centers can be derived from the geometric relationship as follows.

$$\alpha_1 = \pi - \theta + O \tag{7}$$

$$\alpha_2 = \theta - O \tag{8}$$

where α_1 and α_2 are used to denote the case of concave and convex interface shapes, respectively.

Therefore, the comparison of the magnitudes of θ and π for the cases of concave and convex interfaces are considered synthetically to form a unified expression

$$\alpha = \frac{\pi}{2} - \frac{\theta - \pi}{|\theta - \pi|}\left(\frac{\pi}{2} - O\right) - |\theta - \pi| \tag{9}$$

where θ denotes the curvature of interface. According to the law of Sines, we obtain

$$\alpha = \sin^{-1}\left[\frac{\sin O}{D'}\left(\frac{D'}{2} + \frac{\theta - \pi}{|\theta - \pi|}\left(h_L - \frac{D}{2}\right)\right)\right] \tag{10}$$

By combining the diameter of interface circle and angle of the center of circle, the perimeter of the gas–liquid interface can be calculated as follows:

$$S_i = D'|\theta - \pi| = \frac{D\sin(O)|\theta - \pi|}{\sin|\theta - \pi|} \tag{11}$$

The wetting perimeter of the liquid phase was calculated by multiplying the pipe circle diameter by the interface angle, as follows:

$$S_L = D \cdot O \tag{12}$$

The gas–liquid interface characteristics near the pipe wall can be captured by calculating the wet perimeter. Furthermore, the gas-wetting perimeter can be determined as follows:

$$S_G = \pi D - S_L \tag{13}$$

The main intersection points in the double-circle model are replaced by letters N_1, N_2, N_3 and N_4 to facilitate the description of geometric relationships, as shown in Fig. 23. The expression for the cross-sectional

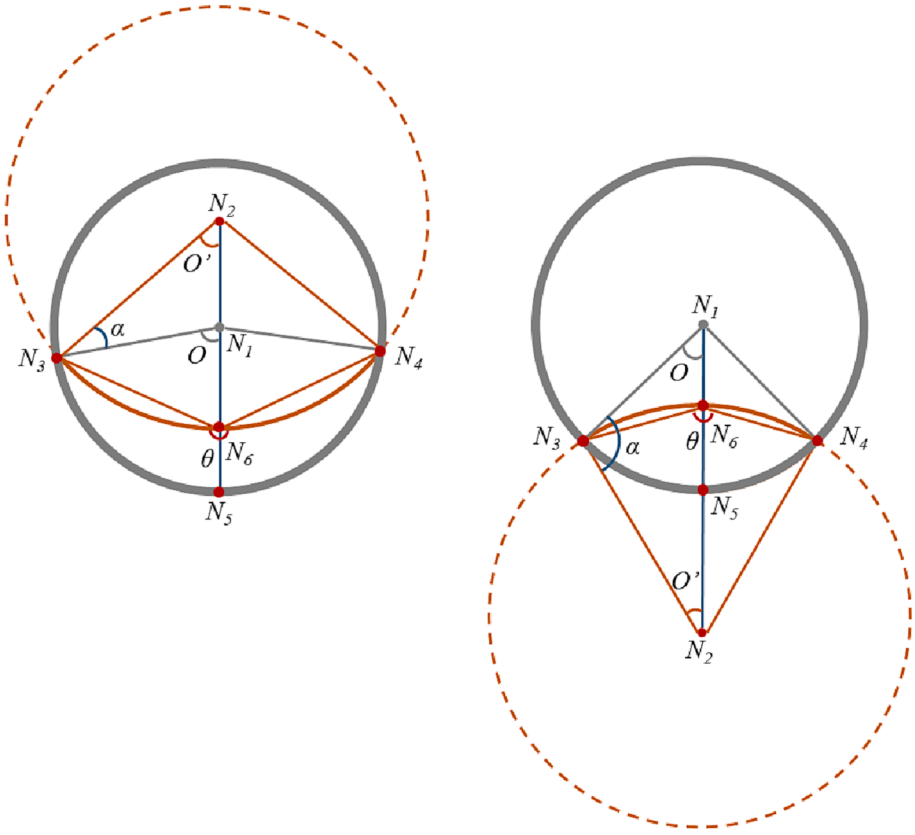

Fig. 23. Schematic of gas–liquid interface.

area occupied by the liquid phase in the stratified flow can be derived by calculating the area of the sector and triangle. A deeper analysis of the geometrical relationships leads to the derivation of an expression for the cross-sectional area occupied by the liquid phase (A_L) in stratified flow, as follows:

$$A_L = A_S - \left|2S_\Delta - A_S^{'}\right| \tag{14}$$

$$2S_\Delta = \left[\frac{D^{'}}{2} + \frac{\theta-\pi}{|\theta-\pi|}\left(h_L - \frac{D}{2}\right)\right]\frac{D}{2}\sin(O) \tag{15}$$

where A_S and A_S' represent the sector area of pipe circle and sector area of the curved circle under the current interface shape, respectively. Specifically, A_S denotes the area of the sector consisting of N_1, N_3, N_4, N_5, and A_S' denotes the area of the sector consisting of N_2, N_3, N_4, N_6. In addition, S_Δ denotes the area of the triangle consisting of N_1, N_2 and N_3 whose values are equal to the area of the triangle consisting of N_1, N_2 and N_4, both of which are expressed by S_Δ. Thus,

$$A_S = \frac{S_L \cdot D}{4} \tag{16}$$

$$A_S^{'} = \frac{S_i \cdot D^{'}}{4} \tag{17}$$

3.1. Construction of shape function of gas–liquid interface

The limitations of the models proposed in the previous studies owing to the assumption of an approximate plane was analyzed to explain the causes of interface curvature changes from the mechanism; thus, the gas–liquid interface characteristics of stratified flow can be accurately predicted. Here, a dimensional analysis based on the experimental data was performed to reveal the dominant factor affecting the gas–liquid interface angle. In general, the angle of gas–liquid interface is influenced by many factors, such as the superficial gas velocity, superficial liquid velocity, viscosity of the gas and liquid, and density of the gas and liquid. The general function of the gas–liquid interface angle is expressed as follows:

$$O = f(U_{SL}, \rho_L, \mu_L, U_{SG}, \rho_G, \mu_G, \sigma, D, g, \beta) \tag{18}$$

Table 5 summarizes these variables, corresponding symbols, and dimension.

Four basic physical quantities were selected: U_{SL}, ρ_L, D, g. The influence parameters were combined and transformed based on the dimensional analysis, as presented in Appendix A. The experimental results were used to obtain a significant linear correlation between the interface angle and its related parameters in double logarithmic coordinates. Therefore, the interface angle prediction relation is proposed as

$$O = r\left(\frac{Re_G}{Re_L}\right)^l We^t \left(\frac{1}{X}\right)^s \left[1 - \frac{\beta}{180}\pi\right]^w \tag{19}$$

Table 5
Summary of variable information.

Variable	Symbol	Dimension		
		M	L	T
Angle of gas–liquid interface	O	—	—	—
Superficial liquid velocity	U_{SL}		1	−1
Density of liquid	ρ_L	1	−3	
Viscosity of liquid	μ_L	1	−1	−1
Superficial liquid velocity	U_{SG}		1	−1
Density of gas	ρ_G	1	−3	
Viscosity of gas	μ_G	1	−1	−1
Surface tension coefficient of gas–liquid	σ	1		−2
Diameter of pipe	D		1	
Gravitational acceleration	g		1	−2
Pipe inclination angle	β	—	—	—

The ordinary-least-squares technique was applied to fit the correction factors to the interface angle function, as expressed in Eq. (19), using the experimental test data. The interface angle function was fitted using experimental data from 263 sets of stratified flows in the horizontal and inclined pipes, and the following equation was obtained:

$$O = 1.39\left(\frac{Re_{SG}}{Re_{SL}}\right)^{-0.29} We^{-0.05}\left(\frac{1}{X}\right)^{0.14}\left[1-\frac{\beta\pi}{180}\right]^{-11.12} \tag{20}$$

Additionally, the interface angle model was evaluated. The results revealed that the error was within 20%, as shown in Fig. 24. Indeed, more than 80% of the data had an error of 15% or less, which is acceptable for predictions. Since there are few tests in the published literature for the parameters related to the interface angle, it is difficult to seek a data set that can be used to evaluate the predictive performance of the interface angle function proposed in this work; therefore, the predicted results are briefly compared with the experimental data of this work here. However, the generalizability evaluation for the model will be systematically compared with the test and finding of other researchers in the subsequent section in the form of a complete reproduction of the interface shape calculation.

3.2. Solutions for stratified flow model with 3D nonflat interface

In the establishment of the nonplanar model, the interface bending in the cross-sectional dimensions of the pipe and interface fluctuations in the flow direction were comprehensively considered to guarantee a realistic analysis of an actual flow state. Fig. 25 shows a schematic of the nonflat stratified flow structure in the pipe.

Furthermore, it is assumed that both gas–liquid phases are incompressible fluids. However, this assumption differs from that in the actual situation. As the employed fluid flows in the pipe, the gas continuously expands as the pressure gradually decreases, leading to a gradual increase in the velocity of gas phase, which is accompanied by a change in the pressure gradient. Therefore, the conventional two-fluid model, as presented in Appendix B, was further supplemented and optimized by introducing an acceleration pressure drop to achieve the construction of 3D flow characteristics in the pipeline.

Based on the two-fluid model, the momentum balance equation for gas–liquid stratified flow can be solved by combining the geometric model, interface shape function, and acceleration pressure drop to obtain a prediction model for the flow characteristic parameters, such as the liquid height at the center of cross-section, average liquid retention, and interface fluctuation. Thus, the 3D nonflat stratified flow volume

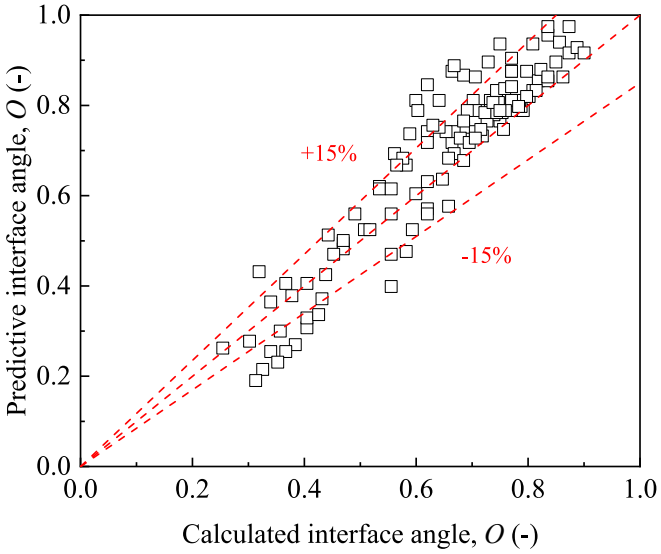

Fig. 24. Prediction effect of interface angle.

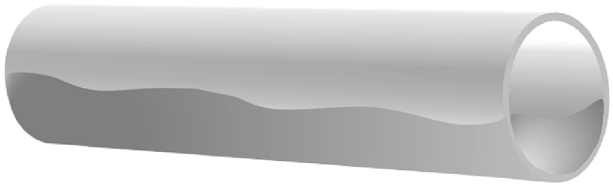

Fig. 25. Schematic diagram of the flow structure.

equation can be expressed as

$$-A_L\left(\frac{dP}{dx}\right)_{TP} - \tau_L S_L + \tau_i S_i + \rho_L A_L g\sin\beta = \frac{d(m_L u_L)}{dx} \tag{21}$$

$$-A_G\left(\frac{dP}{dx}\right)_{TP} - \tau_G S_G - \tau_i S_i + \rho_G A_G g\sin\beta = \frac{d(m_G u_G)}{dx} \tag{22}$$

$$\tau_G\frac{S_G}{A_G} - \tau_L\frac{S_L}{A_L} + \tau_i S_i\left(\frac{1}{A_L}+\frac{1}{A_G}\right) + (\rho_L-\rho_G)g\sin\beta = \frac{1}{A_L}\frac{d(m_L u_L)}{dx} - \frac{1}{A_G}\frac{d(m_G u_G)}{dx} \tag{23}$$

The solution methods for the gas / liquid-wall shear stress and interface shear stress are referred to as the conventional two-fluid stratified flow model, as presented in Appendix A.

The ratio of the interface friction to the gas wall friction is widely used to characterize the interface effect in the study of stratified flow. Many semi-empirical expressions for the interfacial friction factor were introduced with the assumption of a smooth flat interface (Cohen and Hanratty, 1968; Crowley et al., 1992; Kowalski, 1987; Taitel and Dukler, 1976; Ullmann et al., 2003). However, this approach introduces errors that are particularly neglected at fluctuations and flow transition, where obvious ripple and amplitude waves can exist. In conjunction with the work of Rodriguez and Baldani (2012), several interfacial friction models applicable to wavy flow (Andritsos and Hanratty, 1987; Kowalski, 1987; Wallis, 1969) were compared for the prediction error of interfacial shear with the help of experimental data from this work. The results show that the Wallis' model is effective in predicting the interfacial shear for nonplanar stratified flows and that the model integrates the effects of fluctuation amplitude and air-wall friction factor. Therefore, the prediction model for the interfacial friction factor, proposed by Wallis, was used in this study. This model considers the case of a nonplanar steady state of the interface and introduces the dimensionless parameter of the fluctuation amplitude, which is expressed as follows:

$$f_i = f_G\left(1 + C\frac{\delta}{D}\right) \tag{24}$$

where δ denotes the amplitude of fluctuations at the stratified flow interface and C is a parameter determined using experimental tests.

In addition, for the acceleration pressure-drop term on the right-hand side of Eq. (23), a theoretical derivation was performed using the gas–liquid phase velocity differential equation and gas equation of state, as described in Appendix C.

The parameters in Eq. (23) are dimensionless owing to employing the dimensional analysis method; in addition, relevant parameters are introduced for the solution. The final two-phase momentum balance equation is expressed as follows:

$$\frac{\widetilde{S}_G\cdot\widetilde{u}_G^{2-n_G}}{\widetilde{A}_G\cdot\widetilde{D}_G^{n_G}} - X^2\cdot\frac{\widetilde{S}_L\cdot\widetilde{u}_L^{2-n_L}}{\widetilde{A}_L\cdot\widetilde{D}_L^{n_L}} + \widetilde{P}\cdot\frac{\widetilde{S}_i\cdot\widetilde{u}_G^{2-n_G}}{\widetilde{A}_G\cdot\widetilde{A}_L\cdot\widetilde{D}_G^{n_G}}\cdot\left(1-q\frac{\widetilde{u}_L}{\widetilde{u}_G}\right)\cdot\left|1-q\frac{\widetilde{u}_L}{\widetilde{u}_G}\right| + 4\widetilde{Y} + \widetilde{W}\cdot\left[\frac{Re_G}{(1-\varepsilon)^2}+\frac{Re_L}{\varepsilon^2}\right] - \widetilde{J}\cdot\Phi_G^2\cdot(1-\varepsilon) = 0 \tag{25}$$

where X^2 and Φ_G^2 are parameters defined by Lockhart-Matinelli (1949), and $\widetilde{P}, \widetilde{W}, \widetilde{J}$ are newly defined dimensionless parameters.

$$X^2 = \frac{(dP/dx)_{SL}}{(dP/dx)_{SG}} \tag{26}$$

$$\Phi_G^2 = \frac{(dP/dx)_{TP}}{(dP/dx)_{SG}} \tag{27}$$

$$\widetilde{Y} = \frac{(\rho_L - \rho_G)g\sin(\beta\pi/180)}{(dP/dx)_{SG}} \tag{28}$$

$$\widetilde{P} = \frac{\pi}{4}\frac{f_i}{f_G} \tag{29}$$

$$\widetilde{W} = \frac{D}{32}\frac{d\varepsilon}{dx} \tag{30}$$

$$\widetilde{J} = \frac{U_{SG}^2}{RT} \tag{31}$$

where for Newtonian fluids, the expressions for the frictional pressure drop in the gas and liquid phases involved in Eq. (26) are

$$(dP/dx)_{SG} = \frac{\tau_G S}{A} = \frac{32\mu_G U_{SG}}{D^2} \tag{32}$$

$$(dP/dx)_{SL} = \frac{\tau_L S}{A} = \frac{32\mu_L U_{SL}}{D^2} \tag{33}$$

where $d\varepsilon/dx$ in Eq. (30) represents variations in the average liquid holdup of the cross-section in the flow direction, which can be obtained from the experimental data for the two electrode planes of ERT. Thus,

$$\frac{d\varepsilon}{dx} = \frac{\varepsilon_P' - \varepsilon_P}{L_P' - L_P} \tag{34}$$

where ε_P' and ε_P are the average liquid holdups measured at the second and first electrode planes, respectively. The corresponding L_P' and L_P represent the positions of the second and first electrode planes, respectively.

Each parameter in Eq. (25) can be expressed as a function of the interface angle O and interface curvature angle θ, where the interface angle can be solved using the construction method described in Subsection 3.1. Therefore, the final form of Eq. (25) is only a function of θ, and the two-phase momentum balance equation of gas–liquid stratified flow can be solved by introducing the corresponding parameters of the incoming flow conditions.

Moreover, combining Eqs. (9) and (10) yields the liquid height at the center of pipe section, h_L, as a function of the curvature of the interface, as follows:

$$h_L = \frac{D'/2\cdot\sin(\alpha)/\sin(O) - D'/2}{(\theta-\pi)/|\theta-\pi|} + \frac{D}{2} \tag{35}$$

where D′ represents the diameter of virtual circle formed by the interface, which is calculated according to the triangle Sine theorem, as expressed in Eq. (5).

The area occupied by the liquid phase at the pipe interface can be solved by substituting Eqs. (15)–(17) into Eq. (14); thus, the area occupied by the gas phase can be obtained as follows:

$$A_G = A - A_L \tag{36}$$

Therefore, Eq. (24) can be reduced to only contain the interface curvature parameter; thus, it can be solved for a defined incoming flow condition.

With the definition of liquid holdup and above solution, the prediction model of holdup in a gas–liquid stratified flow under the nonplanar assumption can be obtained as follows:

$$\varepsilon = \frac{A_L}{A} = \frac{A_S - |2S_\Delta - A_S'|}{A} = \frac{1}{\pi}\left(O - \left|\frac{\sin^2 O(\sin^2\alpha - |\theta-\pi|)}{\sin^2|\theta-\pi|}\right|\right) \tag{37}$$

In addition, the total pressure gradient of the two-phase stratified flow is calculated as

$$\begin{aligned}(dP/dx)_{TP} = \frac{RT(1-\varepsilon)}{U_{SG}^2 - RT(1-\varepsilon)}\cdot\Bigg\{&\frac{(dP/dx)_{SL}}{\pi}\widetilde{u}_L^{2-n_L}\widetilde{D}_L^{-n_L}\widetilde{S}_L \\ &+ \frac{(dP/dx)_{SG}}{\pi}\widetilde{u}_G^{2-n_G}\widetilde{D}_G^{-n_G}\widetilde{S}_G - [\rho_L\varepsilon + \rho_G(1-\varepsilon)]g\sin(\frac{\beta\pi}{180}) \\ &+ \frac{d\varepsilon}{dx}\left[\frac{\rho_G U_{SG}^2}{(1-\varepsilon)^2} - \frac{\rho_L U_{SL}^2}{\varepsilon^2}\right]\Bigg\}\end{aligned} \tag{38}$$

The function of the interface angle O in Eq. (25) is determined using Eq. (20), whereas the angle α corresponding to the line connecting the centers of pipe and virtual interface circles is expressed by Eq. (9), which are functions of interface curvature. Therefore, the interface curvature under a certain operating condition is obtained by solving the momentum equation (Eq. (25)), which is then substituted into Eqs. (35) and (37) to obtain a prediction of liquid height at the center of cross-section and liquid holdup in the gas–liquid stratified flow. Fig. 26 shows the implemented iterative scheme.

4. Evaluation of the nonflat interface stratified flow model

The validity of the model was verified using experimental data based on the proposed model for predicting the interface of stratified flow. In particular, the prediction of liquid height, prediction effect of the gas–liquid interface shape in the pipe cross-section, and interface fluctuation in the flow direction were evaluated. In addition, the performance of proposed model was compared with that of other models presented in previous studies, and the reasons for the discrepancies and model improvements were analyzed.

4.1. Interface shape of pipe cross-section

The proposed nonflat interface stratified flow model was solved to obtain gas–liquid interface characteristics of the pipeline cross-section under defined operating conditions, considering parameters such as the liquid surface height at the center of pipeline and degree of interface curvature. The prediction results of the model were compared with the experimental results of the cross-sectional parameters and those presented by Ullmann and Brauner (2006). In addition, the prediction effect of the proposed nonflat model was evaluated.

Fig. 27 shows a comparison of the model predictions and experimental test results for the shape of the gas–liquid stratified interface in a horizontal pipe, where the red hollow dots represent the experimental data, black solid line represents our model prediction results, and black dashed line indicates the results using the model presented by Ullmann and Brauner (2006). The experimental data showed that in the horizontal pipe, the liquid height at the center of pipe decreases with an increasing superficial gas velocity. Simultaneously, the curvature of gas–liquid interface decreases, and the interface shape transitions from an obvious concave to a flat shape, which is also reflected in the results of the flow characterization presented in Subsection 4.2. Nevertheless, in the inclined downward stratified flow, the gas–liquid interface exhibited a clear convex trend, as shown in Fig. 28. The nonflat stratified flow computational model provides valid predictions in terms of both the liquid height and interface shape. A valuable description of the degree of interface bending influenced by the gas phase velocity is expressed in terms of the shape curvature.

Consequently, the proposed stratified flow prediction model can reasonably predict the interface characteristics under the nonflat assumption, particularly in the region beyond 0.2 D from the wall. This

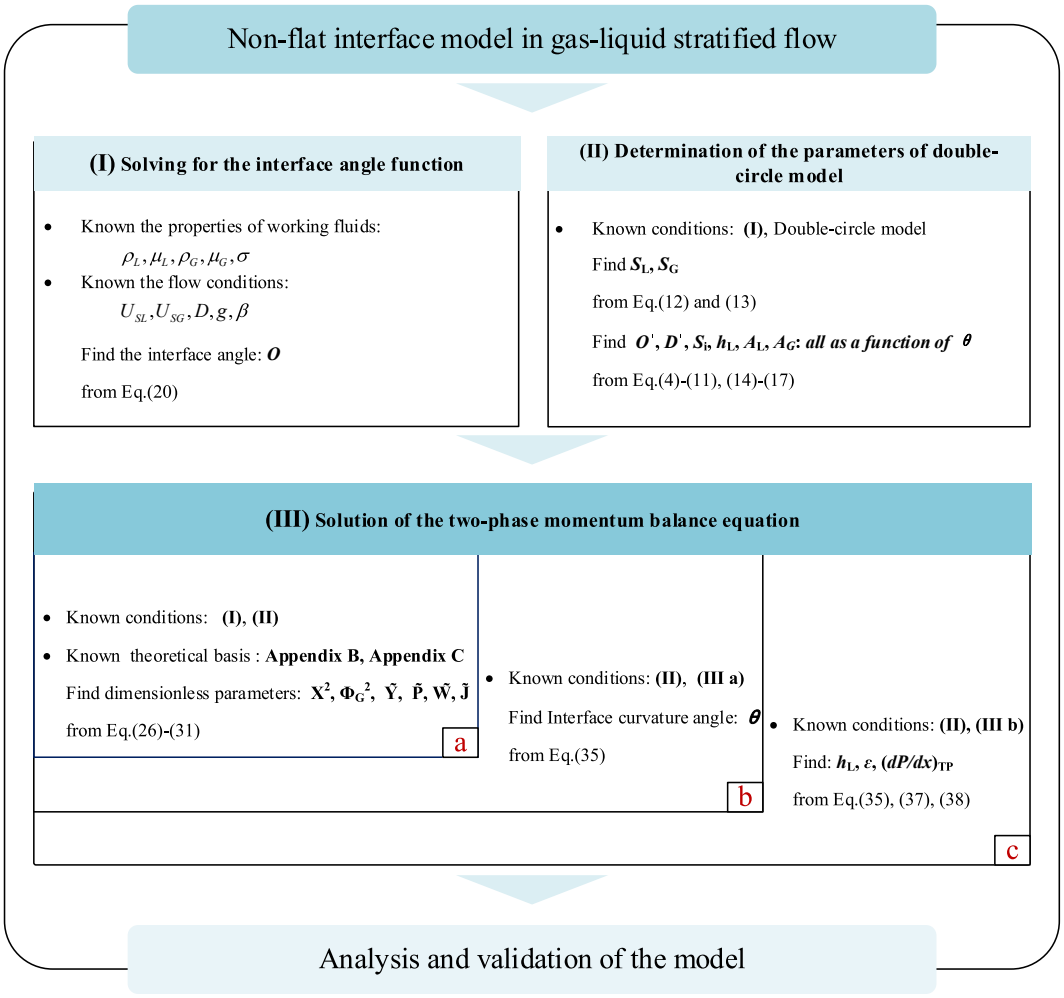

Fig. 26. Block diagram of the algorithm to calculate the nonplanar hierarchical flow model.

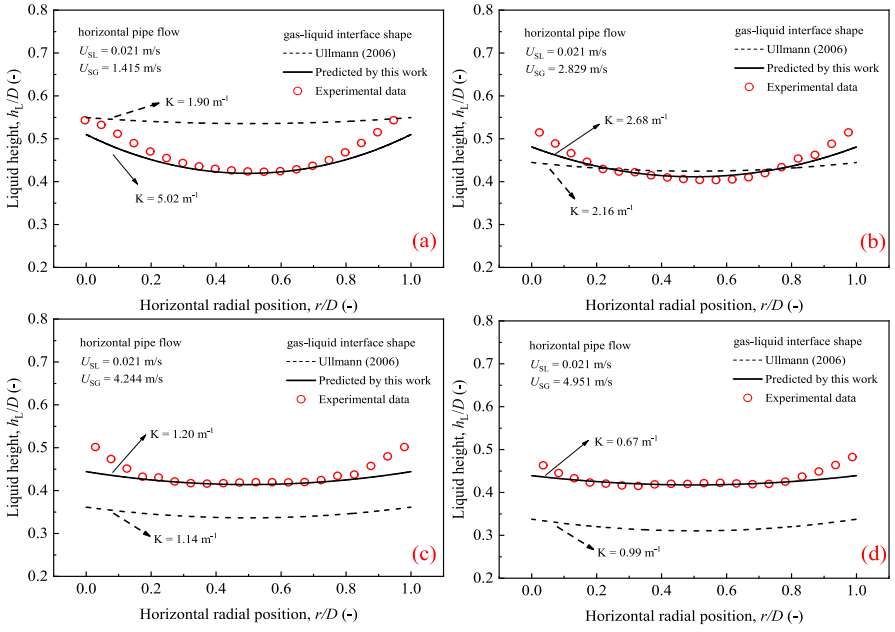

Fig. 27. Validation of interface characteristics in the horizontal stratified flow.

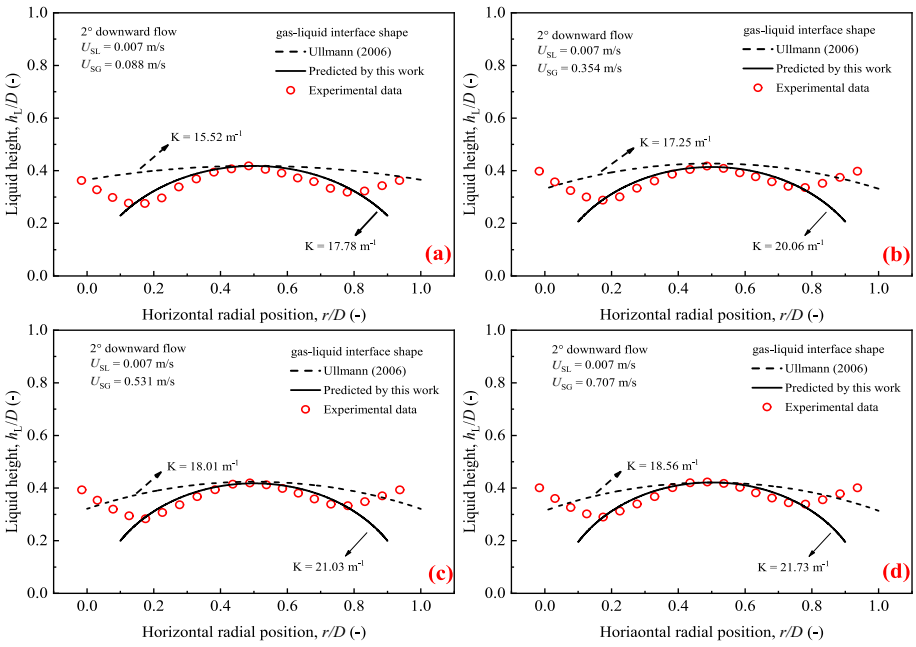

Fig. 28. Validation of interface characteristics in the downward stratified flow.

is because the established interface model is based on a simple double-circle geometry; therefore, the model has a reasonable descriptiveness of the bending trend and degree of the stratified flow interface in the cross-section, whereas it cannot predict the complex curve in a small area near the wall caused by sidewall climbing.

The comparison results show that the interface prediction model proposed in this work is superior in the pipeline cross-sectional direction, evaluated in terms of both liquid surface height and interface bending curvature. Specifically, as shown in Fig. 27, the new model represented by the solid line is closer to the experimental data in terms of liquid height. Meanwhile, Fig. 28 reveals that the new model fits the experimental test results more closely in curvature. However, the model introduced by Ullmann et al. (2006) can effectively predict the phase holdup and pressure drop for nonflat stratified flow under certain operating conditions; but for the working conditions of Figs. 27 and 28, their model has some limitations in predicting the central liquid level height in horizontal flow and the degree of interface bending in inclined stratified flow. The reason for this may be the empirical relationship between the introduced interface angle and interface curvature angle, or the present experimental conditions are beyond their applicability.

The analysis results show that the prediction of the interface shape model for the liquid height at the center of pipe cross-section satisfactorily agrees with the experimental results; And the proposed model in this work can capture changes in the interface bending shape caused by variations in the incoming flow conditions in the horizontal pipe more accurately and provide the interface shape curvature quantitatively.

4.2. *Interfacial fluctuations in the flow direction*

The experimental study revealed that the stratified flow interface exhibits regular fluctuations in the flow direction, which is caused by the acceleration pressure drop that occurs during the flow. The pulsation of the liquid height at the center of pipe at different moments can be obtained by integrating the acceleration pressure drop term into the non-flat stratified flow model and finding the solution. The calculated values using the proposed model were compared with the experimentally tested liquid heights, and the prediction confidence of interfacial fluctuations in the flow direction was discussed.

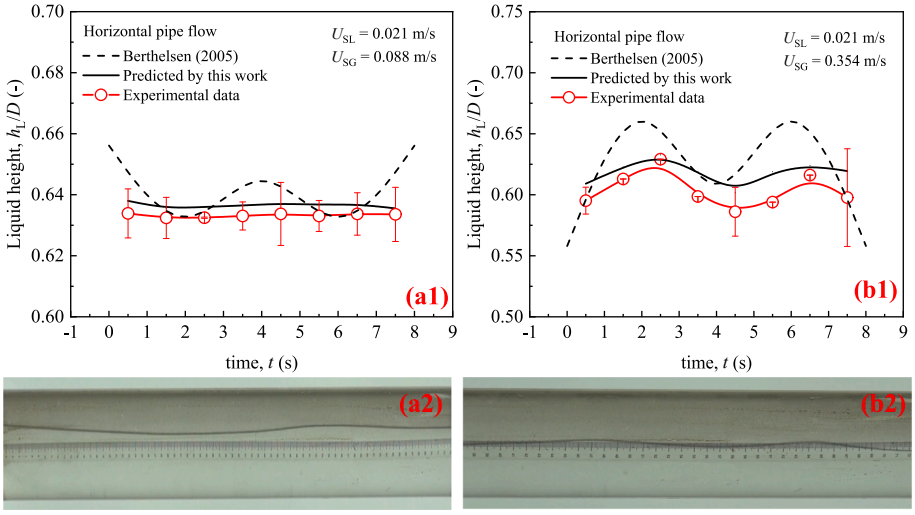

Fig. 29. Fluctuation of stratified flow interface under a low gas–liquid ratio in the horizontal pipe.

The interface fluctuations under different operating conditions and corresponding visualized experimental records are shown in Figs. 29 and 30, which present fluctuations for the low and high gas-to-liquid ratios, respectively. The red dotted line represents measured liquid height, black solid line indicates the predicted values using the proposed model, and black dashed line indicates the results presented by Berthelsen and Ytrehus (2005). The experimental data were averaged using the results of three replicate experiments; test errors are indicated by the error bars.

The results show that the gas–liquid interface is not stable and constant at different moments under the same operating conditions; however, it fluctuates in a certain range around the equilibrium value. In addition, the frequency and amplitude of the interface significantly fluctuations differed under different incoming flow conditions.

The proposed model introduces an acceleration pressure drop for the solution and considers the time dependence of the cross-sectional inclusion rate change within a flow cycle. The model can yield a better prediction of the interfacial fluctuations in the flow direction and variations in the liquid surface height, which satisfactorily agrees with the experimental data, as shown in Fig. 31. In addition, the results obtained using the model proposed by Berthelsen and Ytrehus (2005) with equivalent roughness instead of interfacial fluctuations show that the model generally overestimates the amplitude of interfacial fluctuations compared with the experimental results; this it cannot describe the time-varying effects. Meanwhile, the experimental images visualize the fluctuation of interface, which agrees with the model calculation results.

Variations in the gas–liquid interface in the flow direction reveal that the prediction results using the proposed model reasonably agree with those of the experiments. In addition, Figs. 29–31 show the variation pattern of the liquid height with a variable gas–liquid velocity, which agrees with the experimental result. Meanwhile, the experimental images visualize the fluctuation of interface, which is consistent with the results obtained using the proposed model.

5. Conclusions

In this study, the interface characteristics and influencing factors of gas–liquid stratified flow in pipelines were investigated. Based on the experimental data and theoretical analysis, the calculation function of the gas–liquid stratified flow interface in the pipe was proposed, and the two–phase stratified flow model was modified considering the interface shape and acceleration pressure drop. In contrast to the traditional stratified flow model, the model is able to systematically predict the interface information in the two investigated dimensions of pipe cross-sectional direction and flow direction, including the interface curvature, gas–liquid interface position and interface fluctuations in the flow direction, which contributes to a profound exploration of the characteristics of stratified flows; in particular, it provides a solution for the description of 3D characteristics of the interface.

The obtained results of gas–liquid stratified flow revealed that concave or convex nonplanar structural features are prevalent at the interface and exhibit significant fluctuations in the flow direction. Moreover, velocity of fluids and pipe inclination angles can change the degree and direction of bending of the stratified flow interface in the pipe. A critical gas–liquid ratio determines the interfacial shape transition, which is approximately 200 and 5 in the horizontal and inclined downward pipelines, respectively. The factors influencing the interface shape of stratified flow were further examined by constructing the interface shape function using the dimensional analysis. Additionally, in a gas/liquid stratified flow system, the gas velocity in a high liquid holdup condition directly increases interfacial fluctuations in the flow direction. However, in the low liquid holdup case, the gas occupies the cross-sectional space, leading to a decrease in the liquid height and gradual transformation of interfacial fluctuations into high-frequency small ripples. According to the experimental and theoretical analyses, the acceleration pressure drop that forms the interfacial fluctuation is introduced into the stratified flow solution to form a 3D nonplanar stratified flow calculation model.

Based on the two-fluid theoretical model and indoor experimental data, a nonplanar gas–liquid stratified flow calculation model was modified, considering the shape of stratified interface in the pipe cross-section and interface fluctuations in the flow direction. In addition, a prediction method for 3D characteristics of the stratified interface was proposed. Validation of the experimental data showed that the proposed model could predict the stratified flow interface characteristics. In general, although the proposed model has some limitations, it helps explore the formation mechanism and influencing factors of gas–liquid interfaces in stratified flow systems and provides a research idea for analyzing the interface characteristics from a 3D perspective.

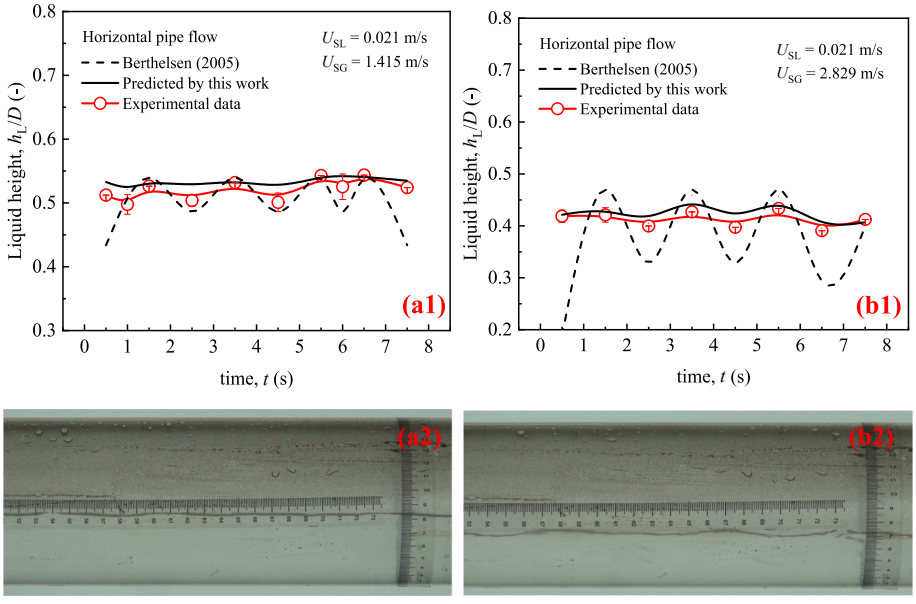

Fig. 30. Fluctuation of stratified flow interface under a high gas–liquid ratio in the horizontal pipe.

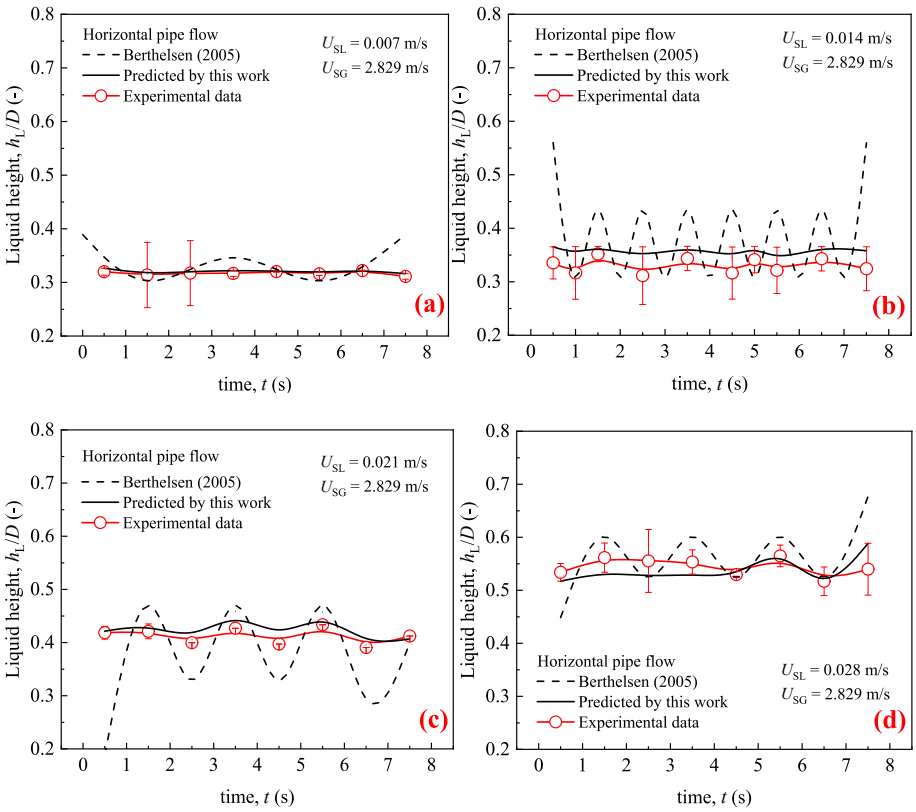

Fig. 31. Variation of interfacial fluctuations at the superficial liquid velocity.

Declaration of Competing Interest

The authors declare that they have no known competing financial interests or personal relationships that could have appeared to influence the work reported in this paper.

Data availability

The authors do not have permission to share data.

Acknowledgments

This work present was supported by the National Natural Science Foundation of China (Grant No: 12102436).

Appendix A:. Procedure for establishing the interface angle function

According to the basic principle of dimensional analysis (Buckingham, 1914), several dimensionless PI parameters (Π) can be obtained as follows:

$$\Pi_1 = O \tag{A1}$$

$$\Pi_2 = \frac{\mu_L}{\rho_L U_{SL} D} \tag{A2}$$

$$\Pi_3 = \frac{U_{SG}}{U_{SL}} \tag{A3}$$

$$\Pi_4 = \frac{\rho_G}{\rho_L} \tag{A4}$$

$$\Pi_5 = \frac{\mu_G}{\rho_L U_{SL} D} \tag{A5}$$

$$\Pi_6 = \frac{\sigma}{\rho_L U_{SL}^2 D} \tag{A6}$$

They were integrated to form simplified and widely used dimensionless parameters. The operational process is as follows:

$$\Pi_7 = \frac{\Pi_3 \cdot \Pi_4}{\Pi_5} = \frac{\rho_G U_{SG} D}{\mu_G} \tag{A7}$$

$$\Pi_8 = \frac{\Pi_6}{(1-\Pi_4)(\Pi_3-1)^2} = \frac{\sigma}{(\rho_L-\rho_G)(U_{SG}-U_{SL})^2 D} \tag{A8}$$

$$\Pi_9 = \sqrt{\Pi_3 \cdot \overset{2}{\underset{4}{\Pi}}} = \sqrt{\frac{\rho_G}{\rho_L}\cdot\left(\frac{U_{SG}}{U_{SL}}\right)^2} \tag{A9}$$

$$\Pi_{10} = \beta \tag{A10}$$

Therefore, the general form of dimensionless expression function, including all parameters, is as follows:

$$\Pi_1 = f(\Pi_2, \Pi_7, \Pi_8, \Pi_9, \Pi_{10}) \tag{A11}$$

$$O = f\left(\frac{1}{Re_L}, Re_G, \frac{1}{We}, \sqrt{\frac{\rho_G}{\rho_L}\cdot\left(\frac{U_{SG}}{U_{SL}}\right)^2}, \beta\right) \tag{A12}$$

Appendix B:. Two-fluid model for smooth stratified flow

For gas–liquid stratified flow, the existing predictive models are essentially one-dimensional models based on the momentum balances of both phases (Ishii and Hibiki, 2006; Barnea and Taitel, 1989; Ishii and Mishima, 1984; Ishii, 1975). Assuming a completely developed stratified flow and equal pressure gradients in both phases, the integral forms of the momentum equations for the two phases are written as follows:

$$-A_L\left(\frac{dP}{dx}\right)_{TP} - \tau_L S_L + \tau_i S_i + \rho_L A_L g\sin\beta = 0 \tag{B1}$$

$$-A_G\left(\frac{dP}{dx}\right)_{TP} - \tau_G S_G - \tau_i S_i + \rho_G A_G g\sin\beta = 0 \tag{B2}$$

where the subscripts *TP*, *L*, *G*, and *i* refer to the two-phase, liquid-phase, gas-phase, and interface, respectively. A_L and A_G are the cross-sectional areas of the pipe occupied by liquid and gas phases, respectively. τ_L, τ_G, and τ_i are the shear stresses at the wall-liquid, wall-gas, and gas–liquid interfaces, respectively. In addition, S_L, S_G, and S_i are the contact parameters of the liquid-wall, gas-wall, and gas–liquid interfaces, respectively, ρ is the density, g is the acceleration owing to gravity, and β represents the pipe inclination (rad).

Various stresses in terms of friction factors can be defined and widely used as follows (Taitel and Dukler, 1976)

$$\tau_G = f_G\cdot\frac{\rho_G u_G^2}{2} \tag{B3}$$

$$\tau_L = f_L\cdot\frac{\rho_L u_L^2}{2} \tag{B4}$$

$$\tau_i = f_i\cdot\frac{\rho_G(u_G-u_L)|u_G-u_L|}{2} \tag{B5}$$

where u is the average velocity and f is the friction factor in the smooth pipe of each phase.

The curvature of interface can be further solved by dimensionless treatment of the above parameters and integrating them back into the momentum equations of the gas–liquid stratified flow. In the solution process, the friction factors of the air and liquid walls are calculated as follows:

$$f_L = C_L Re_L^{-n_L} \tag{B6}$$

$$f_G = C_G Re_G^{-n_G} \tag{B7}$$

where $C_L = C_G = 16, n_L = n_G = 1$ for laminar flow, $C_L = C_G = 0.046, n_L = n_G = 0.2$ for turbulent flow (Bishop and Deshpande, 1986; Lioumbas et al., 2007; Xu et al., 2007).

The Reynolds number for the gas phase as Newtonian fluid is defined as

$$Re_{L,G} = \frac{\rho_{L,G} u_{L,G} D_{L,G}}{\mu_{L,G}} \tag{B8}$$

where D_L and D_G are the equivalent diameters of the liquid and gas phases, respectively, which can be obtained from the area occupied by the phase and contact perimeter.

$$D_L = \frac{4A_L}{S_L} \tag{B9}$$

$$D_G = \frac{4A_G}{S_G + S_i} \tag{B10}$$

Normalizing the parameters in Eqs. (B1) and (B2) yields

$$\widetilde{D}_G = D_G/D \tag{B11}$$

$$\widetilde{D}_L = D_L/D \tag{B12}$$

$$\widetilde{S}_G = S_G/D \tag{B13}$$

$$\widetilde{S}_L = S_L/D \tag{B14}$$

$$\widetilde{S}_i = S_i/D \tag{B15}$$

$$\widetilde{A}_G = A_G/D^2 \tag{B16}$$

$$\widetilde{A}_L = A_L/D^2 \tag{B17}$$

The local phase velocity $\widetilde{u}_{G,L}$ is normalized with respect to the superficial velocity of each phase, $U_{SG,\ SL}$, and $q = U_{SL}/U_{SG}$. All dimensionless quantities with a tilde (~) in the above equations are functions of the dimensionless liquid height. Using the mass conservation equation, the dimensionless velocity can be expressed as

$$\widetilde{u}_G = u_G/U_{SG} = \frac{\pi}{4}\widetilde{A}_G^{-1} \tag{B18}$$

$$\widetilde{u}_L = u_L/U_{SL} = \frac{\pi}{4}\widetilde{A}_L^{-1} \tag{B19}$$

Appendix C:. Acceleration pressure drop

The acceleration pressure drop for multiphase flow in a nonvariable cross-sectional pipeline is considered to be caused by gas expansion. Although in the study of gas–liquid layered flow, it is assumed that both gas–liquid phases are incompressible fluids, this assumption differs from the actual situation. When the fluid flew in the pipe, a gradual decrease of the pressure continuously expanded the gas, resulting in a gradual increase in the velocity of gas phase, which was accompanied by a change in the pressure gradient.

The acceleration pressure drop is expressed as (Beggs and Brill, 1973)

$$-\left(\frac{dP}{dx}\right)_a = \frac{1}{A}\frac{d}{dx}(m_L u_L + m_G u_G) \tag{C1}$$

where $-(dP/dx)_a$ denotes the acceleration pressure drop and m is the mass flow rate. The mass flow rate of each phase can be calculated using the phase holdup as follows:

$$m_L = \rho_L \varepsilon A u_L \tag{C2}$$

$$m_G = \rho_G (1-\varepsilon) A u_G \tag{C3}$$

where the relationship between the phase velocity and superficial velocity satisfies

$$u_L = \frac{U_{SL}A}{A_L} = \frac{U_{SL}}{\varepsilon} \tag{C4}$$

$$u_G = \frac{U_{SG}A}{A_G} = \frac{U_{SG}}{1-\varepsilon} \tag{C5}$$

Therefore, the acceleration pressure drop can be expressed as

$$-\left(\frac{dP}{dx}\right)_a = \rho_L U_{SL}\frac{du_L}{dx} + \rho_G U_{SG}\frac{du_G}{dx} \tag{C6}$$

Mathematical transformations help write

$$\frac{du_L}{dx} = \frac{d}{dx}\left(\frac{U_{SL}}{\varepsilon}\right) = \frac{\varepsilon(dU_{SL}/dx) - U_{SL}(d\varepsilon/dx)}{\varepsilon^2} = -\frac{U_{SL}(d\varepsilon/dx)}{\varepsilon^2} \tag{C7}$$

$$\frac{du_G}{dx} = \frac{d}{dx}\left(\frac{U_{SG}}{1-\varepsilon}\right) = \frac{(1-\varepsilon)(dU_{SG}/dx) + U_{SG}(d\varepsilon/dx)}{(1-\varepsilon)^2} \tag{C8}$$

The gas mass conservation yields

$$\frac{\partial \rho_G}{\partial t} + \frac{\partial(\rho_G U_{SG})}{\partial x} = 0 \tag{C9}$$

The assumption of a constant flow satisfies

$$\frac{\rho_G dU_{SG}}{dx} + \frac{U_{SG}d\rho_G}{dx} = 0 \tag{C10}$$

In addition, the state equation of gas under adiabatic conditions yields

$$PM = \rho RT \tag{C11}$$

where M is the molar mass of substance, R is the gas constant (287 J/kg·K), and T is the absolute temperature (293.15 K at room temperature). Under adiabatic conditions, the differential form of Eq. (C11) can be expressed as

$$\frac{d\rho_G}{dx} = \frac{1}{RT}\frac{dP}{dx} \tag{C12}$$

where dP/dx is the total pressure gradient in the pipeline.

Finally, the acceleration pressure drop can be expressed as

$$-\left(\frac{dP}{dx}\right)_a = \frac{d\varepsilon}{dx}\left[\frac{\rho_G U_{SG}^2}{(1-\varepsilon)^2} - \frac{\rho_L U_{SL}^2}{\varepsilon^2}\right] - \frac{U_{SG}^2}{RT(1-\varepsilon)}\frac{dP}{dx} \tag{C13}$$

References

Andritsos, N., 1992. Statistical analysis of waves in horizontal stratified gas-liquid flow. Int. J. Multiphase Flow 18 (3), 465–473. https://doi.org/10.1016/0301-9322(92)90029-G.

Andritsos, N., Hanratty, T.J., 1987. Interfacial instabilities for horizontal gas–liquid flows in pipelines. Int. J. Multiphase Flow 13, 583–603. https://doi.org/10.1016/0301-9322(87)90037-1.

Banafi, A., Talaie, M.R., 2020. A new mechanistic model to predict gas–liquid interface shape of gas–liquid flow through pipes with low liquid loading. AIChE J. 61 (3), 1043–1053. https://doi.org/10.1016/j.ngib.2019.12.005.

Barnea, D.A., 1987. A unified model for predicting flow-pattern transitions for the whole range of pipe inclinations. Int. J. Multiphase Flow 13 (1), 1–12. https://doi.org/10.1016/0301-9322(87)90002-4.

Barnea, D., 1991. On the effect of viscosity on stability of stratified gas liquid flow—application to flow pattern transition at various pipe inclinations. Chem. Eng. Sci. 46, 2123–2131. https://doi.org/10.1016/0009-2509(91)80170-4.

Barnea, D., Taitel, Y., 1989. Transient-formulation modes and stability of steady-state annular flow. Chem. Eng. Sci. 44, 325–332. https://doi.org/10.1016/0009-2509(89)85069-9.

Barnea, D., Taitel, Y., 1993. Kelvin-Helmholtz stability criteria for stratified flow, viscous versus non-viscous (inviscid) approaches. Int. J. Multiphase Flow 19, 639–649. https://doi.org/10.1016/0301-9322(93)90092-9.

Barnea, D., Taitel, Y., 1994. Non-linear interfacial instability of separated flow. Chem. Eng. Sci. 49, 2341–2349. https://doi.org/10.1016/0009-2509(94)E0047-T.

Barral, A.H., Angeli, P., 2013. Interfacial characteristics of stratified liquid–liquid flows using a conductance probe. Exp. Fluids 54, 1604. https://doi.org/10.1007/s00348-013-1604-5.

Beggs, H.D., Brill, J.P., 1973. A study of two-phase flow in inclined pipes. J. Petrol. Technol. 25 (5), 607–617.

Belden, J., Techet, A.H., 2011. Simultaneous quantitative flow measurement using PIV on both sides of the air—water interface for breaking waves. Exp. Fluids 50, 149–161. https://doi.org/10.1007/s00348-010-0901-5.

Berthelsen, P.A., Ytrehus, T., 2005. Calculations of stratified wavy two-phase flow in pipes. Int. J. Multiphase Flow 31, 571–592. https://doi.org/10.1016/j.ijmultiphaseflow.2005.02.001.

Berthelsen, P.A., Ytrehus, T., 2007. Stratified smooth two-phase flow using the immersed interface method. Comput. Fluids 36 (7), 1273–1289. https://doi.org/10.1016/j.compfluid.2007.01.002.

Bevington, P.R., Robinson, O.K., 2003. Data Reduction and Error Analysis for the Physical Sciences, 3rd ed. McGraw-Hill Press, Boston, pp. 39–40.

Birvalski, M., Tummers, M.J., Delfos, R., Henkes, R.A.W.M., 2013. PIV measurements of waves and turbulence in stratified horizontal two-phase pipe flow. In: 10th Int. Symp. on Particle Image Velocimetry, A099, Delft, The Netherlands.

Birvalski, M., Tummers, M.J., Delfos, R., Henkes, R.A.W.M., 2014. PIV measurements of waves and turbulence in stratified horizontal two-phase pipe flow. Int. J. Multiphase Flow. 62, 161–173. https://doi.org/10.1016/j.ijmultiphaseflow.2014.03.001.

Bishop, A.A., Deshpande, S.D., 1986. Non-Newtonian liquid-air stratified flow through horizontal tubes-II. Int. J. Multiphase Flow 12, 977–996. https://doi.org/10.1016/0301-9322(86)90038-8.

Bolton, G., Bennett, M., Wang, M., Qiu, C., Wright, M., Primrose, K., Stanley, S., Rhodes, D., 2007. Development of an electrical tomographic system for operation in a remote, acidic and radioactive environment. Chem. Eng. J. 130 (2-3), 165–169.

Brauner, N., Rovinsky, J., Moalem Maron, D., 1995b. Analytical solution of laminar stratified flow with curved interfaces. In: Proceedings of the NURETH-7 Meeting ANS, 1, 192-211. https://doi.org/10.2172/106991.

Brauner, N., Rovinsky, J., Moalem Maron, D., 1995a. Analytical solution for laminar-laminar two–phase stratified flow in circular conduits. Chem. Eng. Commun. 141–142, 103–143. https://doi.org/10.1080/00986449608936412.

Brauner, N., Rovinsky, J., Moalem Maron, D., 1996. Determination of the interface curvature in stratified two-phase systems by energy considerations. Int. J. Multiphase Flow 22, 1167–1185. https://doi.org/10.1016/0301-9322(96)00046-8.

Brauner, N., Moalem Moran, D., Rovinsky, J., 1998. A two-fluid model for stratified flows with curved interfaces. Int. J. Multiphase Flow 24, 975–1004. https://doi.org/10.1016/S0301-9322(98)00005-6.

Buckingham, E., 1914. On physically similar systems; illustrations of the use of dimensional equations. Phys. Rev. 4 (4), 345–376. https://doi.org/10.1103/PhysRev.4.345.

Chen, X., Cai, X., Brill, J.P., 1997. Gas–liquid stratified wavy flow in horizontal pipelines. ASME J. Energy Resour. Technol. 119 (4), 209–216. https://doi.org/10.1115/1.2794992.

Cherdantsev, A.V., Zdornikov, S.A., Cherdantsev, M.V., Isaenkov, S.V., Markovich, D.M., 2022. Stratified-to-annular gas–liquid flow patterns transition in a horizontal pipe. Exp. Therm. Fluid Sci. 132, 110552 https://doi.org/10.1016/j.expthermflusci.2021.110552.

Cohen, S.L., Hanratty, T.J., 1968. Effects of waves at a gas–liquid interface on a turbulent air flow. J. Fluid Mech. 3, 467–469. https://doi.org/10.1017/S0022112068000285.

Crowley, C.J., Wallis, G.B., Barry, J.J., 1992. Validation of a one-dimensional wave model for the stratified-to-slug flow regime transition, with consequences for wave growth and slug frequency. Int. J. Multiphase Flow. 18 (2), 249–271. https://doi.org/10.1016/0301-9322(92)90087-W.

Dong, F., Tan, C., Liu, J., Xu, Y., Wang, H., 2006. Development of single drive electrode electrical resistance tomography system. IEEE Trans. Instrum. Meas. 55 (4), 1208–1214.

Fernandino, M., Ytrehus, T., 2008. Effect of interfacial waves on turbulence structure in stratified duct flows. J. Fluid Eng. – T. ASME. 130, 061201(1–8). https://doi.org/10.1115/1.2928295.

Geselowitz, D.B., 1971. An application of electrocardiographic lead theory to impedance plethysmography. IEEE Trans. Biomed. Eng. 18 (1), 38–41.

Gorelik, D., Brauner, N., 1999. The interface configuration in two-phase stratified pipe flows. Int. J. Multiphase Flow 25 (6–7), 977–1007. https://doi.org/10.1016/S0301-9322(99)00038-5.

Grue, J., Jensen, A., Rusas, P., Sveen, J., 1999. Properties of large-amplitude internal waves. J. Fluid Mech. 380, 257–278. https://doi.org/10.1017/S0022112098003528.

Guo, W., Liu, C., Wang, L., Huang, R., 2020. Response of thermal diffusion to gas–liquid stratified/wave flow and its application in measurement. Chem. Eng. Sci. 225, 115789 https://doi.org/10.1016/j.ces.2020.115789.

Hudaya, A.Z., Widyatama, A., Dinaryanto, O., Juwana, W.E., Indarto, D., 2019. The liquid wave characteristics during the transportation of air-water stratified co-current two-phase flow in a horizontal pipe. Exp. Therm. Fluid Sci. 103, 304–317. https://doi.org/10.1016/j.expthermflusci.2019.01.021.

Ishii, M., Hibiki, T., 2006. Thermo-fluid dynamics of two-phase flow. Springer, US, https://doi.org/10.1007/978-0-387-29187-1.

Ishii, M., Mishima, K., 1984. Two-fluid model and hydrodynamic constitutive relations. Nucl. Eng. Des. 82, 107–126. https://doi.org/10.1016/0029-5493(84)90207-3.

Ishii, M., 1975. Thermo-fluid dynamic theory of two-phase flow. Collection de la Direction des Etudes et Researches d'Electricite de France, Eyrolles, Paris, France.

Katopodes, N. D., 2019. "Chapter 2—Air-water interface" in Free-Surface Flow. London, U.K. Butterworth, 44-121. https://www.sciencedirect.com/science/article/pii/B9780128154878000020.

Kowalski, J.E., 1987. Wall and interfacial shear stress in stratified flow in a horizontal pipe. AIChE J. 33 (2), 274–281. https://doi.org/10.1002/aic.690330214.

Kumar, K., Fershtman, A., Barnea, D., Shemer, L., 2021. Evolution of waves in a horizontal pipe propagating on a surface of a liquid film sheared by gas. Phys. Fluids 33 (6), 062115. https://doi.org/10.1063/5.0049288.

Li, H., Wang, M., Wu, Y.X., Lucas, G., 2009. Volume flow rate measurement in vertical oil-in-water pipe flow using electrical impedance tomography and a local probe. Multiphase Sci. Technol. 21 (1–2), 81–93. https://doi.org/10.1615/MultScienTechn.v21.i1-2.70.

Li, K., Wang, Q., Wang, M., 2019a. Three-dimensional visualisation of gas-water two-phase flow based on bubble mapping method and size projection algorithm. Flow Meas. Instrument. 69, 101590 https://doi.org/10.1016/j.flowmeasinst.2019.101590.

Li, K., Wang, Q., Wang, M., Han, Y., 2019b. Imaging of a distinctive large bubble in gas–water flow based on a size projection algorithm. Meas. Sci. Technol. 30 (9), 094004. https://doi.org/10.1088/1361-6501/ab16b0.

Lin, M., Moeng, C., Tsai, W., Sullivan, P.P., Belcher, S.E., 2008. Direct numerical simulation of wind-wave generation processes. J. Fluid Mech. 616, 1–30. https://doi.org/10.1017/S0022112008004060.

Lioumbas, J.S., Mouza, A., Paras, S.V., Karabelas, A.J., 2007. Liquid layer characteristics in stratified gas–liquid downflow: a study of transition to wavy flow. Heat Transfer Eng. 28, 625–632. https://doi.org/10.1080/01457630701266447.

Murai, T., Kagawa, Y., 1985. Electrical impedance computed tomography based on a finite element model. IEEE Trans. Biomed. Eng. 32, 177–184. https://doi.org/10.1109/TBME.1985.325526.

Ng, T.S., Lawrence, C.J., Hewitt, G.F., 2001. Interface shapes for two-phase laminar stratified flow in a circular pipe. Int. J. Multiphase Flow 27 (7), 1301–1311. https://doi.org/10.1016/S0301-9322(01)00005-2.

Ong, J., Enden, G., Popel, A.S., 1994. Converging three-dimensional Stokes flow of two fluids in a T-type bifur- cation. J. Fluid Mech. 270, 51–72. https://doi.org/10.1017/S0022112094004192.

Pitton, E., Ciandri, P., Margarone, M., Andreussi, P., 2014. An experimental study of stratified–dispersed flow in horizontal pipes. Int. J. Multiphase Flow 67, 92–103. https://doi.org/10.1016/j.ijmultiphaseflow.2014.05.018.

Rashidi, M., Banerjee, S., 1988. Turbulence structure in free surface channel flows. Phys. Fluids 31, 2491–2503. https://doi.org/10.1063/1.866603.

Rodriguez, O.M.H., Baldani, L.S., 2012. Prediction of pressure gradient and holdup in wavy stratified liquid–liquid inclined pipe flow. J. Petrol Sci. Eng. 96–97, 140–151. https://doi.org/10.1016/j.petrol.2012.09.007.

Sanjou, M., Nezu, I., 2011. Turbulence structure and coherent vortices in open-channel flows with wind-induced waves. Environ. Fluid Mech. 11, 113–131. https://doi.org/10.1007/s10652-011-9210-7.

Taitel, Y., Dukler, A.E., 1976. A model for predicting flow regime transitions in horizontal and near horizontal gas–liquid flow. Am. Inst. Chem. Eng., [Spring Natl. Meet.]. 22, 51–55. https://doi.org/10.1002/aic.690220105.

Tzotzi, C., Bontozoglou, V., Andritsos, N., Vlachogiannis, M., 2011. Effect of fluid properties on flow patterns in two-phase gas–liquid flow in horizontal and downward pipes. Ind. Eng. Chem. Res. 50, 645–655. https://doi.org/10.1021/ie100239v.

Ullmann, A., Brauner, N., 2006. Closure relations for two-fluid models for two-phase stratified smooth and stratified wavy flows. Int. J. Multiphase Flow 32, 82–105. https://doi.org/10.1016/j.ijmultiphaseflow.2005.08.005.

Ullmann, A., Zamir, M., Ludmer, Z., Brauner, N., 2003. Stratified laminar countercurrent flow of two liquid phases in inclined tubes. Int. J. Multiphase Flow 29, 1583–1604. https://doi.org/10.1016/S0301-9322(03)00144-7.

Valle, A., Kvandal, H.K., 1995. Pressure drop and dispersion characteristics of separated oil-water flow. In: Celata, G.P., Shah, R.K. (Eds.), Proc. Int. Symp. on two-phase flow modeling and experimentation, Oct. 9-11, Rome, Italy, vol. 1. Edizioni ETS, 583-591.

Wallis, G.B., 1969. In: One-dimensional two-phase flow. Plenum Press. https://doi.org/10.1002/aic.690160603.

Wang, M., Cilliers, J.J., 1999. Detecting non-uniform foam density using electrical resistance tomography. Chem. Eng. Sci. 54 (5), 707–712. https://doi.org/10.1016/S0009-2509(98)00277-2.

Wang, M., Yin, W., Holliday, N., 2002. A highly adaptive electrical impedance sensing system for flow measurement. Meas. Sci. Technol. 13 (12), 1884–1889. https://doi.org/10.1088/0957-0233/13/12/311.

Wijayanta, S., Indarto, Deendarlianto, Catrawedarma, I.G.N.B., Hudaya, A.Z., 2022. Statistical characterization of the interfacial behavior of the sub-regimes in gas–liquid stratified two-phase flow in a horizontal pipe. Flow. Meas. Instrum. 83, 102107. https://doi.org/10.1016/j.flowmeasinst.2021.102107.

Xu, J., Wu, Y., Shi, Z., Lao, L., Li, D., 2007. Studies on two-phase co-current air/non-Newtonian shear-thinning fluid flows in inclined smooth pipes. Int. J. Multiphase Flow 33, 948–969. https://doi.org/10.1016/j.ijmultiphaseflow.2007.03.008.

Zhan, X., He, Y., Shen, B., Sun, Z., Shi, T., Li, X., 2018. Removal of gas bubbles from highly viscous non-Newtonian fluids using controlled vibration. Chem. Eng. Sci. 185, 76–83. https://doi.org/10.1016/j.ces.2018.04.012.